

DEAD Box 1 Facilitates Removal of RNA and Homologous Recombination at DNA Double-Strand Breaks

Lei Li, Devon R. Germain, Ho-Yin Poon, Matthew R. Hildebrandt, Elizabeth A. Monckton, Darin McDonald, Michael J. Hendzel, Roseline Godbout

Department of Oncology, University of Alberta, Cross Cancer Institute, Edmonton, Alberta, Canada

Although RNA and RNA-binding proteins have been linked to double-strand breaks (DSBs), little is known regarding their roles in the cellular response to DSBs and, if any, in the repair process. Here, we provide direct evidence for the presence of RNA-DNA hybrids at DSBs and suggest that binding of RNA to DNA at DSBs may impact repair efficiency. Our data indicate that the RNA-unwinding protein DEAD box 1 (DDX1) is required for efficient DSB repair and cell survival after ionizing radiation (IR), with depletion of DDX1 resulting in reduced DSB repair by homologous recombination (HR). While DDX1 is not essential for end resection, a key step in homology-directed DSB repair, DDX1 is required for maintenance of the single-stranded DNA once generated by end resection. We show that transcription deregulation has a significant effect on DSB repair by HR in DDX1-depleted cells and that RNA-DNA duplexes are elevated at DSBs in DDX1-depleted cells. Based on our combined data, we propose a role for DDX1 in resolving RNA-DNA structures that accumulate at DSBs located at sites of active transcription. Our findings point to a previously uncharacterized requirement for clearing RNA at DSBs for efficient repair by HR.

DEAD box proteins are a family of putative RNA helicases that function by altering RNA secondary structure. This protein family has been implicated in all aspects of RNA metabolism. The *DEAD box 1* gene (*DDX1*) is a widely expressed gene that is mis-expressed in a number of cancers, including retinoblastoma, neuroblastoma, and breast cancer (1, 2). Knockout of *DDX1* leads to early embryonic lethality in mice and severely reduced fertility in flies (3, 4). *DDX1* is involved in the transport of RNAs from the nucleus to the cytoplasm and regulates cytoplasmic localization of the splicing-regulatory protein KSRP (5). In neurons, *DDX1* resides in RNA-transporting granules, cytoplasmic organelles that regulate the localization and expression of target mRNAs (6, 7). *DDX1* has also been identified as a core subunit of the human tRNA ligase complex which is essential for tRNA splicing (8).

In addition to its roles in RNA metabolism, *DDX1* has been implicated in the cellular response to DNA double-strand breaks (DSBs). Upon treatment of cells with ionizing radiation (IR), *DDX1* rapidly accumulates at a subset of DNA DSBs (~30%), where it forms IR-induced foci that colocalize with γ -H2AX, a marker for DSBs (9). *DDX1* coimmunoprecipitates with the MRN (MRE11-RAD50-NBS1) complex, the early sensor of DNA DSBs, and ATM (*ataxia telangiectasia mutated*) protein, the key transducer of the signaling cascade in response to DSBs (10, 11). DSBs induce *DDX1* phosphorylation in an ATM-dependent manner. Notably, IR-induced *DDX1* foci are lost when cells are treated with RNase H, an enzyme that specifically digests RNA from RNA-DNA hybrids (9). These results suggest that RNA-DNA double-stranded structures are required for the presence and/or retention of *DDX1* at DSBs. In line with this observation, biochemical analysis has shown that *DDX1* can unwind both RNA-RNA and RNA-DNA duplexes (9). Consistent with a role in the cellular response to IR-induced DSBs, *DDX1* has also been reported to regulate the maturation of a subset of DSB-induced microRNAs (12).

There is accumulating evidence indicating that RNAs, particularly RNA-DNA hybrid structures, play a role in DNA damage and genome instability (13–15). Huertas and Aguilera (16) re-

ported that budding yeast mutants that are defective in transcription elongation have elevated levels of RNA-DNA duplexes and increased transcription-associated recombination. These authors proposed that increased recombination is due to enhanced formation of R-loops, RNA-DNA duplex structures formed between nascent RNA and its template DNA. In mammalian cells, Li and Manley (17) demonstrated that inactivation of the splicing factor SF2 results in increased DSB formation, which is also accompanied by abnormal R-loop formation. Genome-wide studies in both yeast and human cells have revealed that mutations that impair mRNA processing lead to elevated numbers of γ -H2AX foci and genome instability (18, 19). Together, these studies suggest that deregulated RNA-DNA hybrid formation during transcription can result in the accumulation of DSBs and genome instability. In addition to triggering DSB formation, recent work by Britton et al. (20) suggests that removal of transcription-coupled R-loops in the vicinity of DNA damage generated by microirradiation (micro-IR) is an integral part of the cellular response to DSBs. However, it is not known whether RNA molecules bind DNA at the site of DSBs during repair and, if so, whether RNA-DNA duplexes can impact repair pathway choice and/or efficiency.

To gain insight into the role of *DDX1* in the DNA DSB response, we have examined the efficiencies of different repair path-

Received 14 July 2016 Returned for modification 15 August 2016

Accepted 17 August 2016

Accepted manuscript posted online 22 August 2016

Citation Li L, Germain DR, Poon H-Y, Hildebrandt MR, Monckton EA, McDonald D, Hendzel MJ, Godbout R. 2016. DEAD box 1 facilitates removal of RNA and homologous recombination at DNA double-strand breaks. *Mol Cell Biol* 36: 2794–2810. doi:10.1128/MCB.00415-16.

Address correspondence to Roseline Godbout, rgodbout@ualberta.ca.

Supplemental material for this article may be found at <http://dx.doi.org/10.1128/MCB.00415-16>.

Copyright © 2016, American Society for Microbiology. All Rights Reserved.

TABLE 1 Sequences of small interfering RNAs used in this study

Designation	Sequence (5'→3')
DDX1 si1	CAGGCUGAAUCUAUCCCAUUGAUCU
DDX1 si2	UACACCAUGUUGUUGUCCAGUAAA
CtIP si1	GGGAACAGCAGAAAGUCCUUCUGA
RAD51 si1	UGGAGCAGCGAUGUUGCUGCUGAU
RNF138 si1	CCUGUGUCAAGAAUCAAU
RNF138 si2	UAGAUGAAGAAACCCAAU

ways in DDX1-depleted cells. We demonstrate a role for DDX1 in homologous recombination (HR), with DDX1 involved in the maintenance of single-stranded DNA (ssDNA) at DSBs once generated by end resection. Importantly, we show that RNA-DNA hybrids accumulate at DSBs upon depletion of DDX1. Our results support a key role for DDX1 in the removal of RNA from DNA-RNA duplex structures during DSB repair, thereby facilitating repair by HR.

MATERIALS AND METHODS

Cell culture, irradiation, drug treatment, and flow cytometry. HeLa, U2OS, and U2OS cells with integrated reporters (DR-green fluorescent protein [DR-GFP], EJ5-GFP, SA-GFP, and EJ2-GFP) (21–23) were cultured in Dulbecco modified Eagle medium (DMEM) (Thermo Fisher Scientific) supplemented with 10% fetal calf serum (FCS), 100 U/ml penicillin, and 100 µg/ml streptomycin. Cells were gamma irradiated using a ¹³⁷Cs irradiator (Shepherd, San Fernando, CA) and allowed to recover at 37°C for the indicated times prior to further analysis. Cells were treated with the following drugs: 100 µM cordycepin (Sigma) for 2 h prior to treatment, 1 µM camptothecin (CPT) (Sigma) for 30 min or 1 h, and 5 µM and 10 µM AG14361 (Selleckchem) for 24 h. U2OS cells were synchronized using a double thymidine block as described previously (24). Cells in S and G₂ phases were examined at 3 and 8 h, respectively, after release from the second round of thymidine block (see Fig. S1 in the supplemental material). Flow cytometry of propidium iodide-stained U2OS and U2OS DR-GFP cells was carried out using FACSCalibur (BD Biosciences) as described previously (24), and data were analyzed using FCS Express (De Novo Software).

siRNA knockdown and generation of an siRNA-resistant DDX1 mutant. Gene knockdown was carried out using Stealth small interfering RNAs (siRNAs) (Life Technologies) or Mission siRNAs (Sigma). siRNA sequences are listed in Table 1. Scrambled siRNAs (Medium GC and Low GC negative controls; Life Technologies) served as negative controls. Transfection of siRNAs was carried out with Lipofectamine RNAiMAX (Life Technologies) at a final siRNA concentration of 10 nM. To obtain the maximum efficiency for DDX1 knockdown, cells were split 72 h after the first round of siRNA transfection and underwent a second round of siRNA transfection prior to analysis.

To generate a DDX1 expression construct that is resistant to DDX1 siRNA1 (si1), silent mutations were introduced into DDX1 cDNA at five nucleotides, i.e., CAAGCCGAGTCCATT (mutated nucleotides are underlined), using QuikChange site-directed mutagenesis (Agilent Technologies). U2OS or U2OS DR-GFP cells were transfected with the hemagglutinin (HA)-tagged DDX1 mutant construct (pcDNA3.1 HA-mDDX1), and stable transfectants were selected by growing the cells in 800 µg/ml G418 (Life Technologies) for 2 weeks. Stable transfectants were maintained in medium supplemented with 200 µg/ml G418.

DNA repair assays. The GFP-based DSB repair assays were performed as described previously (21, 23) with modifications. Briefly, U2OS cells with reporters were first transfected with DDX1, RAD51, CtIP, or scrambled siRNAs using Lipofectamine RNAiMAX reagent. Five million cells were then electroporated with 10 µg of pCBA *Sc*e or control plasmids together with 100 pmol of DDX1, RAD51, CtIP, or scrambled siRNA

using a GenePulser II electroporator (Bio-Rad) (280 V, 975 µF). The percentage of GFP-positive cells was quantified by flow cytometry 48 h after electroporation (BD FACSCalibur).

To overexpress transcripts homologous to the upstream region of the I-SceI cut site, a 302-bp fragment located immediately upstream of the I-SceI site was generated by PCR and was cloned into the pcDNA3.1 vector in both orientations to generate sense and antisense RNA transcripts. Genomic DNA from U2OS DR-GFP cells served as the template for PCR amplification of the 302-bp fragment. The following primers were used for PCR: sense forward, 5'ATAAAGCTTAGCGGCGTGCTGACACC3'; sense reverse, 5'GATCTCGAGTATCCCTAGCCGGACACG3'; antisense forward, 5'GATCTCGAGAGCGGCGTGCTGAGCACC3'; and antisense reverse, 5'ATAAAGCTTTATCCCTAGCCGGACACG3'. The pcDNA3.1 vector contains a bovine growth hormone polyadenylation signal that serves as a transcription terminator, ensuring that no vector sequence will be transcribed along with the 302-nucleotide (nt) transcripts. Five micrograms of DNA (pcDNA3.1 302-bp construct or empty vector) was electroporated along with 8 µg of pCBA *Sc*e into control or DDX1 knockdown U2OS DR-GFP cells. GFP-positive cells were quantified as described above.

Micro-IR. Microirradiation (micro-IR) was performed using a spinning-disc confocal microscope (Yokogawa Corp., Japan). Cells were incubated with 10 µM bromodeoxyuridine (BrdU) for 48 h prior, followed by microirradiation with a 405-nm laser and a 40× objective (20% power and 30 iterations). Cells were allowed to recover at 37°C for 1 h prior to immunostaining. Approximately 40 to 80 cells were microirradiated for each condition in each experiment, with three independent experiments performed.

Whole-cell lysates, nuclear extracts preparation, and Western blot analysis. Whole-cell lysates were prepared by resuspending cells in lysis buffer (50 mM Tris-HCl [pH 7.5], 150 mM NaCl, 0.5% sodium deoxycholate, 1% NP-40, and 1× Complete protease inhibitors). Fifty micrograms of lysates was resolved by SDS-PAGE, transferred to nitrocellulose membranes, and immunoblotted with the antibodies indicated below. To generate nuclear extracts, cells were incubated on ice with nucleus isolation buffer (25 mM HEPES [pH 7.9], 250 mM sucrose, 150 mM NaCl, 1.5 mM MgCl₂, 0.2 mM CaCl₂, 0.1% NP-40, 1× PhosSTOP phosphatase inhibitor, and 1× Complete protease inhibitors) for 10 min, followed by centrifugation at 5,000 × *g* for 5 min at 4°C. Pellets were then lysed in nucleus extraction buffer (25 mM HEPES [pH 7.9], 250 mM sucrose, 50 mM NaCl, 1 mM EGTA, 3 mM MgCl₂, 0.5% NP-40, 1× PhosSTOP phosphatase inhibitor, and 1× Complete protease inhibitors). Twenty-five micrograms of extracts was resolved in SDS-PAGE and immunoblotted.

The following antibodies were used for Western blot analysis: rabbit anti-DDX1 (batch 2910, 1:5,000) (25), mouse antiactin (1:20,000; Sigma), rabbit anti-RAD51 (1:500; Santa Cruz), mouse anti-CtIP (1:500; Active Motif), rabbit anti-RNF138 (1:1,000; ProSci), rabbit anti-phospho-RPA32(S4/S8) (1:1,000; Bethyl), mouse anti-replication protein A (anti-RPA) (1:500; Abcam), rabbit anti-phospho-Chk1(S345) (1:1,000; Cell Signaling), and mouse anti-Chk1 (1:1,000; Santa Cruz).

Clonogenic survival assay. To examine sensitivity to the poly(ADP-ribose) polymerase (PARP) inhibitor AG14361, U2OS cells underwent two rounds of DDX1 or control siRNA transfection. Cells were trypsinized 48 h after the second round of transfection, diluted to the same density, and plated in triplicate. The drug was added to the plates on the following day, and cells were exposed to the drug for 24 h. The cells were then washed with phosphate-buffered saline (PBS) and fresh medium added. Nine days after drug treatment, the cells were washed with PBS and stained with 1% crystal violet in 70% ethanol for 30 min at room temperature. The plates were rinsed with water and colonies counted using a Colcount colony counter (Oxford Optronix), with 30 cells as the cutoff. For colony formation upon IR treatment, U2OS cells were transfected with DDX1 or control siRNAs as described above. Cells were plated and gamma irradiated on the same day. Ten days after IR, the cells were washed with PBS and stained as described above.

Fluorescence microscopy. Cells adhering to coverslips were fixed and processed as previously described (9). The following antibodies were used for immunostaining: rabbit anti-53BP1 (1:300; Santa Cruz), mouse anti-BrdU (1:50; Roche), rabbit anti-CENP-F (1:1,000; a gift from Gordon Chan), mouse anti-CtIP (1:200; Active Motif), rabbit anti-DDX1 (batch 2923, 1:1000) (25), rabbit anti-phosphorylated EXO1 (anti-pEXO1) (1:500; a gift from Kum Kum Khanna), mouse anti- γ -H2AX (1:4,000; Upstate Biotechnology), rabbit anti-RAD51 (1:100; Santa Cruz), mouse anti-RNA-DNA hybrid (S9.6) (1:100; a gift from Stephen Leppa), and mouse anti-RPA (1:200; Abcam). For immunostaining analysis, cells were incubated with primary antibodies for 1 h at room temperature, followed by Alexa Fluor 488- and Alexa Fluor 555-conjugated secondary antibodies (Life Technologies) for 1 h at room temperature. Coverslips were mounted onto slides in polyvinyl alcohol (Calbiochem)-based mounting medium containing 1 μ g/ml 4',6'-diamidino-2-phenylindole (DAPI). Immunofluorescence images were captured on a Zeiss LSM710 confocal laser scanning microscope with a plan-Apochromat 63 \times (numerical aperture [NA], 1.4) or 40 \times (NA, 1.3) oil immersion lens using ZEN software. Images were exported as TIFF files using ZEN and assembled using Photoshop software.

The nondenaturing BrdU staining protocol was adapted from that described by Buonomo et al. (26). Briefly, U2OS cells were labeled with 10 μ M BrdU (Sigma) for 24 h. Cells were treated with Triton X-100 buffer (0.5% Triton X-100, 50 mM NaCl, 3 mM MgCl₂, and 300 mM sucrose in PBS) for 10 min at 4°C. Cells were then fixed in 2% paraformaldehyde for 10 min at room temperature and permeabilized in Triton X-100 buffer for 10 min at 4°C. For immunostaining with RPA antibody, cells were treated with CSK buffer [10 mM piperazine-*N,N'*-bis(2-ethanesulfonic acid) (PIPES) (pH 6.8), 300 mM sucrose, 100 mM NaCl, 3 mM MgCl₂, 0.5% Triton X-100, and 1 \times Complete protease inhibitor (Roche)] for 5 min at 4°C. Cells were then fixed in 4% paraformaldehyde, followed by permeabilization in 0.5% Triton X-100.

For quantification of foci, confocal microscope images were captured and analyzed with Imaris software (version 7.7.2; Bitplane AG, Switzerland). A median filter (3X3X1) was applied to reduce background noise. The same signal threshold was applied to all images taken from the same experiment to obtain the numbers of foci in each cell. The intensity threshold values were determined by comparing numbers of foci remaining with the number of clear-cut foci present in confocal images. A minimum of 100 cells were analyzed for each condition tested in each experiment, with each experiment carried out three times unless otherwise specified.

DRIP analysis at the I-SceI cut site. U2OS DR-GFP cells were transfected with DDX1 or control siRNAs. Twenty-four hours after the second round of siRNA transfection, cells were transfected with the pcDNA3.1 HA-ER-I-SceI construct using polyethylenimine (PEI) (Polysciences Inc.) at a ratio of 5 μ g reagent to 1 μ g DNA. Twenty-four hours after DNA transfection, 4-hydroxytamoxifen (Sigma) was added to a final concentration of 5 μ M. Cells were incubated for 4 h and then harvested. The procedure for preparing nucleic acids for DNA-RNA immunoprecipitation (DRIP) analysis has been reported previously (27). Briefly, nucleic acids (genomic DNA along with RNA) were purified by lysing cell pellets in 1% SDS and digesting the lysates overnight with 300 μ g/ml proteinase K. Nucleic acids were extracted using a neutral-pH phenol-chloroform (1:1) mixture followed by ethanol precipitation. Precipitated nucleic acids were spooled with a glass rod, rinsed in 70% ethanol, and dissolved in Tris-EDTA (TE).

DRIP was performed as described previously (28) with some modifications. Nucleic acids were digested overnight at 37°C using an enzyme cocktail (BsrGI, EcoRI, HindIII, SspI, and XbaI). Digested products were purified with phenol-chloroform and resuspended in TE buffer. Four micrograms of digested nucleic acids was incubated with 10 μ g S9.6 antibody in binding buffer (10 mM Tris-HCl [pH 8.0], 1 mM EDTA, 10 mM NaPO₄, 140 mM NaCl, and 0.05% Triton X-100) overnight at 4°C. Protein G beads were then added and incubated for 2 h at 4°C. Where indi-

TABLE 2 Sequences of primers used in DRIP analysis

PCR type	Designation	Sequence (5'→3')
Conventional	I-SceI forward (cut measurement)	CGTGTGCTGTTATTGTGCTGTCT
	I-SceI reverse (cut measurement)	GACTTGAAGAAGTCGTGCTG
	<i>GAPDH</i> forward	CCCCTTCATTGACCTCAACT
	<i>GAPDH</i> reverse	AGCAGACAGTTATGAACCCG
Quantitative	P1 forward	TCGCCACCATGGTGAGCAAG
	P1 reverse	CGGTGGTGCAGATGAACCTC
	P2 forward	AAGACCCACGAGGCAACAC
	P2 reverse	TCGCTCTGGCTCCTGCTCCT
	P3 forward	TCGCCACCATGGTGAGCAAG
	P3 reverse	GACACGCTGAACCTGTGGC
	<i>GAPDH</i> forward	GAACCAGCACCGATCACCTC
	<i>GAPDH</i> reverse	CCAGCCCAAGGTCTTGAGG
	<i>SNRPN</i> forward	GCCAAATGAGTGAGGATGGT
<i>SNRPN</i> reverse	TCCTCTCTGCCTGACTCCAT	

cated, 4 μ g of digested nucleic acids was treated with either 15 units of RNase H (Affymetrix) or 30 μ g of RNase A (Sigma) in a total volume of 100 μ l overnight at 4°C prior to incubation with S9.6 antibody. Immunoprecipitates were washed in binding buffer three times, followed by elution in 50 mM Tris-HCl (pH 8.0), 10 mM EDTA, 0.5% SDS, and 500 μ g/ml proteinase K for 45 min at 55°C. Eluates were extracted with phenol-chloroform and resuspended in 50 μ l 10 mM Tris-HCl, pH 8.0.

Quantitative PCR (qPCR) was performed with SYBR green qPCR mix (Applied Biological Materials Inc., Canada) following the manufacturer's instructions and analyzed on an ABI 7900HT PCR system (Applied Biosystems). Two microliters of eluate was used for each amplification reaction. Two regions upstream of the I-SceI cut site, P2 and P3, were examined. For each region, the relative enrichment of DNA-RNA hybrids was normalized to the signals obtained from input genomic DNA as well as the *SNRPN* negative-control region, as previously described for DRIP analysis (27–29). The average percent IPs in control (scrambled siRNA-transfected) cells for the *SNRPN* (negative control), P2, and P3 loci were 0.06%, 0.55%, and 2.42%, respectively. The average percent IPs in control cells treated with RNase A were 0.08%, 1.34%, and 2.18% for *SNRPN*, P2, and P3, respectively. The average percent IPs in control cells treated with RNase H were 0.11%, 0.4%, and 1.37% for *SNRPN*, P2, and P3, respectively. Relative increases in qPCR signals at P2 and P3 in DDX1 knock-down versus control cells were calculated as described in the figure legend for both RNase A- and RNase H-treated versus untreated cells. qPCR was also used to measure I-SceI cut efficiency using primers flanking the cut site, which was normalized to the signal at the glyceraldehyde-3-phosphate dehydrogenase (*GAPDH*) gene region. Primer sequences are listed in Table 2. The data shown were obtained from three independent experiments. The *P* value was calculated using the Mann-Whitney test.

DSN and RNase H analysis at the I-SceI cut site. DSBs at the I-SceI site were induced in control or DDX1-depleted U2OS DR-GFP cells and nucleic acid extracted as described above. Duplex-specific nuclease (DSN) digestion of nucleic acids was performed according to the manufacturer's directions. Briefly, 1 μ g of nucleic acid in 1 \times DSN buffer (50 mM Tris-HCl [pH 8.0], 5 mM MgCl₂, 1 mM dithiothreitol [DTT]) was digested with 2 units of DSN (Evrogen, Moscow, Russia) at 60°C for 50 min for analysis of the region upstream of the I-SceI cut site. Digested products were precipitated with ethanol and resuspended in sterile water. Where indicated, 1 μ g of nucleic acid was digested with 10 units of RNase H prior to DSN treatment. Two hundred fifty nanograms of DSN-digested nucleic acid or 50 ng of undigested nucleic acid was used for PCR amplification. Primer sequences are listed in Table 3. PCR conditions were as follows: 94°C for 2 min, followed by 40 cycles of 92°C for 30 s, 55°C for 30 s, and

TABLE 3 Sequences of primers used in RNase H/DSN analysis

Designation	Sequence (5' → 3')
Upstream forward	AAGACCCACGAGGCAACAC
Upstream reverse	GACACGCTGAACCTGTGGC
GAPDH forward	CCCCTTCATTGACCTCAACT
GAPDH reverse	AGCAGACAGTTATGAACCCG

72°C for 30 to 45 s (depending on the length of the amplified region), followed by a 7-min incubation at 72°C. PCR products were resolved in a 2% agarose gel and visualized using ethidium bromide. Band intensity was determined using Photoshop software by measuring the average signal intensity over a fixed area and subtracting the background intensity for each band. For each experiment, we set the DDX1 siRNA value to 1, with control values presented relative to the value for DDX1 siRNA. Data shown were obtained from four independent experiments. The *P* value was calculated using the Student *t* test.

RESULTS

DDX1 contributes to DSB repair and cell survival post-IR. We used small interfering RNAs (siRNAs) to examine whether DDX1 is required for cell survival post-IR. DDX1 levels were significantly reduced in cells transfected with either DDX1 siRNA1 (si1) or siRNA2 (si2) (Fig. 1A). siRNA-transfected cells were exposed to 1 to 4 Gy IR, and cell survival was measured using a colony formation assay. DDX1 depletion greatly decreased cell survival at all doses of IR tested (Fig. 1A). We then compared DSB repair kinetics in control and DDX1-depleted cells using the numbers of γ -H2AX foci as a readout (30). Thirty minutes after treatment with 3 Gy IR, similar numbers of γ -H2AX foci were observed in control and DDX1-depleted cells, indicating that the absence of DDX1 did not affect γ -H2AX focus formation. In contrast, at 4 h, both DDX1 si1- and si2-transfected cells had ~50% more γ -H2AX foci than control cells (Fig. 1B and C), suggesting that DDX1 depletion impaired DSB repair efficiency. This difference disappeared at 24 h postirradiation.

To verify that the reduced efficiency in DSB repair was caused by DDX1 knockdown and not off-target effects of siRNAs, we generated a U2OS cell line that stably expresses HA-tagged siRNA (si1)-resistant DDX1 (U2OS HA-mDDX1) (Fig. 1D). Similar numbers of IR-induced foci were observed in this cell line and in parental U2OS cells (Fig. 1D; see Fig. 2F and 3B). DDX1 knockdown using DDX1 si1 did not result in increased numbers of γ -H2AX foci in HA-expressing cells (Fig. 1D), confirming that delayed DSB repair in DDX1-depleted cells is a consequence of DDX1 depletion. These results indicate that DDX1 is required for efficient DSB repair and cell survival post-IR.

As cells in G₂ phase have twice the DNA and twice the number of DSBs as G₁-phase cells (30–33), we further examined γ -H2AX foci in control and DDX1-depleted cells in G₁ versus G₂ phase. We used centromere protein F (CENP-F) immunostaining to distinguish cells in G₁ (when CENP-F is absent) from those in G₂ (when CENP-F expression peaks) (Fig. 1E) (31, 32, 34). Compared to control cells, DDX1-depleted cells accumulated more γ -H2AX foci in G₂ phase than in G₁ phase at 4 h after IR, with an ~60% increase in foci in G₂ compared to ~40% in G₁ (Fig. 1F). These results indicate that DDX1 makes a stronger contribution to DSB repair in the G₂ phase than in the G₁ phase of the cell cycle.

DDX1 promotes HR-mediated DSB repair. In mammalian cells, the majority of DSBs are repaired by either homologous

recombination (HR) or nonhomologous end joining (NHEJ) (10, 11). It is generally accepted that NHEJ is the predominant pathway for DSB repair in the G₁ phase of the cell cycle, with both HR and NHEJ playing a role in DSB repair during S and G₂ phases (32, 33). Consequently, cells defective in HR usually exhibit more pronounced DSB repair defects in the S and G₂ phases than in G₁ (32, 33). The fact that DDX1 depletion leads to slower DSB repair in G₂- than in G₁-phase cells suggests a role for DDX1 in HR-mediated DSB repair. To investigate this possibility, we used U2OS DR-GFP cells (22) as reporters to measure HR efficiency. When U2OS DR-GFP cells were cotransfected with scrambled siRNA and the I-SceI-encoding expression vector (with I-SceI endonuclease activity generating the DSBs), ~7 to 10% of the cells were GFP positive, indicating that these cells had repaired the I-SceI-induced DSBs through HR. Knockdown of DDX1 with either si1 or si2 reduced homology-directed DSB repair efficiency by 2- to 3-fold (Fig. 2A), suggesting a positive role for DDX1 in HR.

To ensure that the observed effect on HR was indeed due to DDX1 depletion rather than off-target effects, we generated U2OS DR-GFP cells that stably express siRNA-resistant DDX1 (U2OS DR-GFP HA-mDDX1). In these cells, DDX1 siRNA transfection caused only a mild decrease (~20%) in HR efficiency (Fig. 2B). These data are in line with the observation that only 70 to 80% of U2OS DR-GFP HA-mDDX1 cells express HA-mDDX1. As a final test of DDX1 specificity, we examined cell cycle phase distribution in control and DDX1-depleted cells to determine whether the impaired HR observed upon DDX1 depletion might be the consequence of cell cycle disturbance. Similar cell cycle distributions were observed for U2OS and U2OS DR-GFP whether DDX1 was depleted or not and whether the cells were treated with IR or not (see Fig. S2 in the supplemental material), indicating that DDX1's effect on HR is not mediated through cell cycle changes.

Cells defective in HR demonstrate elevated sensitivity to inhibitors of poly(ADP-ribose) polymerase (PARP) (35, 36). We therefore treated control and DDX1-depleted U2OS cells with AG14361, a PARP-1 inhibitor. Knockdown of DDX1 using two different siRNAs resulted in an ~2-fold decrease in colony formation upon treatment with AG14361 at both concentrations tested (Fig. 2C). Taken together, our data indicate a role for DDX1 in efficient HR-mediated DSB repair.

Effect of DDX1 on NHEJ, single-strand annealing and alternative NHEJ. We examined the effect of DDX1 knockdown on the repair of DSBs by NHEJ. U2OS EJ5-GFP cells (21) transfected with DDX1 siRNAs showed slightly elevated NHEJ efficiency compared to control cells (1.4-fold and 1.1-fold, respectively) (Fig. 2D), suggesting that DDX1 does not play a significant role in NHEJ. We also examined whether DDX1 affects two subpathways of DSB repair, single-strand annealing and alternative NHEJ, by using U2OS SA-GFP and U2OS EJ2-GFP cell lines as reporters, respectively (21). Depletion of DDX1 suppressed both pathways by 2- to 4-fold (see Fig. S3 in the supplemental material).

DDX1 is involved in RAD51 focus formation. RAD51 has been specifically linked to DSB repair by HR. We therefore investigated the effect of DDX1 on RAD51 focus formation in U2OS cells upon IR treatment. DDX1 depletion resulted in an ~30% decrease in RAD51 foci compared to control cells (Fig. 2E and F). As RAD51 foci form predominantly in S and G₂ phases (37), we synchronized U2OS cells using a double thymidine block (see Fig. S1 in the supplemental material) and analyzed RAD51 foci in S and G₂ phases in control and DDX1-depleted cells treated with IR.

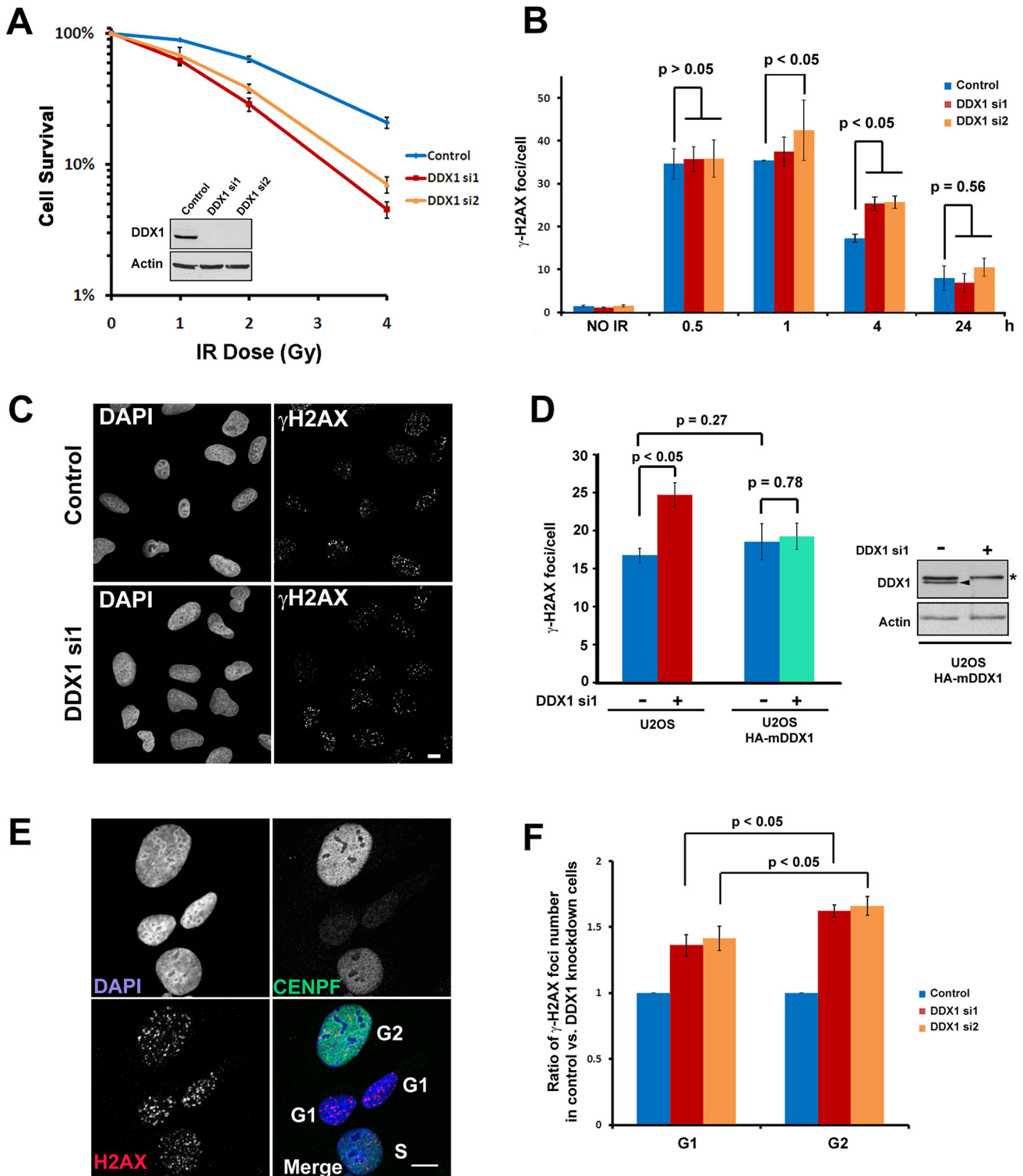


FIG 1 DDX1 promotes cell survival and DSB repair in irradiated cells. (A) U2OS cells transfected with scrambled siRNAs (control) or siRNAs targeting DDX1 (siRNA1 [si1] and siRNA2 [si2]) were exposed to the indicated doses of IR. Cell survival was measured by colony formation assay. Inset, Western blot of U2OS cells transfected with scrambled siRNAs (control) or DDX1 siRNAs. (B) Statistical analysis of average numbers of γ -H2AX foci in control and DDX1 knockdown cells at 0.5, 1, 4, and 24 h after 3 Gy IR. (C) Control and DDX1 knockdown U2OS cells were exposed to 3 Gy IR. Immunostaining with anti- γ -H2AX antibody was performed 4 h post-IR. (D) Left, U2OS and U2OS HA-mDDX1 cells that stably express siRNA-resistant DDX1 were transfected with scrambled (-) or DDX1 (+) siRNA. Numbers of γ -H2AX foci were analyzed 4 h after 3 Gy IR. For U2OS HA-mDDX1 cells, only cells that express HA-mDDX1 (positive for HA staining) were analyzed. Right, Western blot of U2OS HA-mDDX1 cell lysates that were transfected with scrambled siRNAs (-) or DDX1 siRNA (+). The asterisk indicates HA-tagged DDX1 that is resistant to DDX1 siRNA. The arrowhead points to endogenous DDX1. (E) U2OS cells were immunostained with the indicated antibodies 4 h after 3 Gy IR. Cells in different phases of the cell cycle were distinguished by CENP-F intensities: weak, medium, and strong CENP-F immunostaining indicates cells in G₁, S, and G₂ phases, respectively. (F) Numbers of γ -H2AX foci in control and DDX1 knockdown U2OS cells were analyzed 4 h after 3 Gy IR. Cells in G₁ and G₂ phases were distinguished by CENP-F immunostaining intensities. Ratios of γ -H2AX foci in control versus DDX1 knockdown cells in G₁ and G₂ phases are depicted in the graphs. For all samples, $n = 3$; error bars are standard errors of the means (SEM). P values were calculated using the two-sided Student t test. Scale bars, 10 μ m.

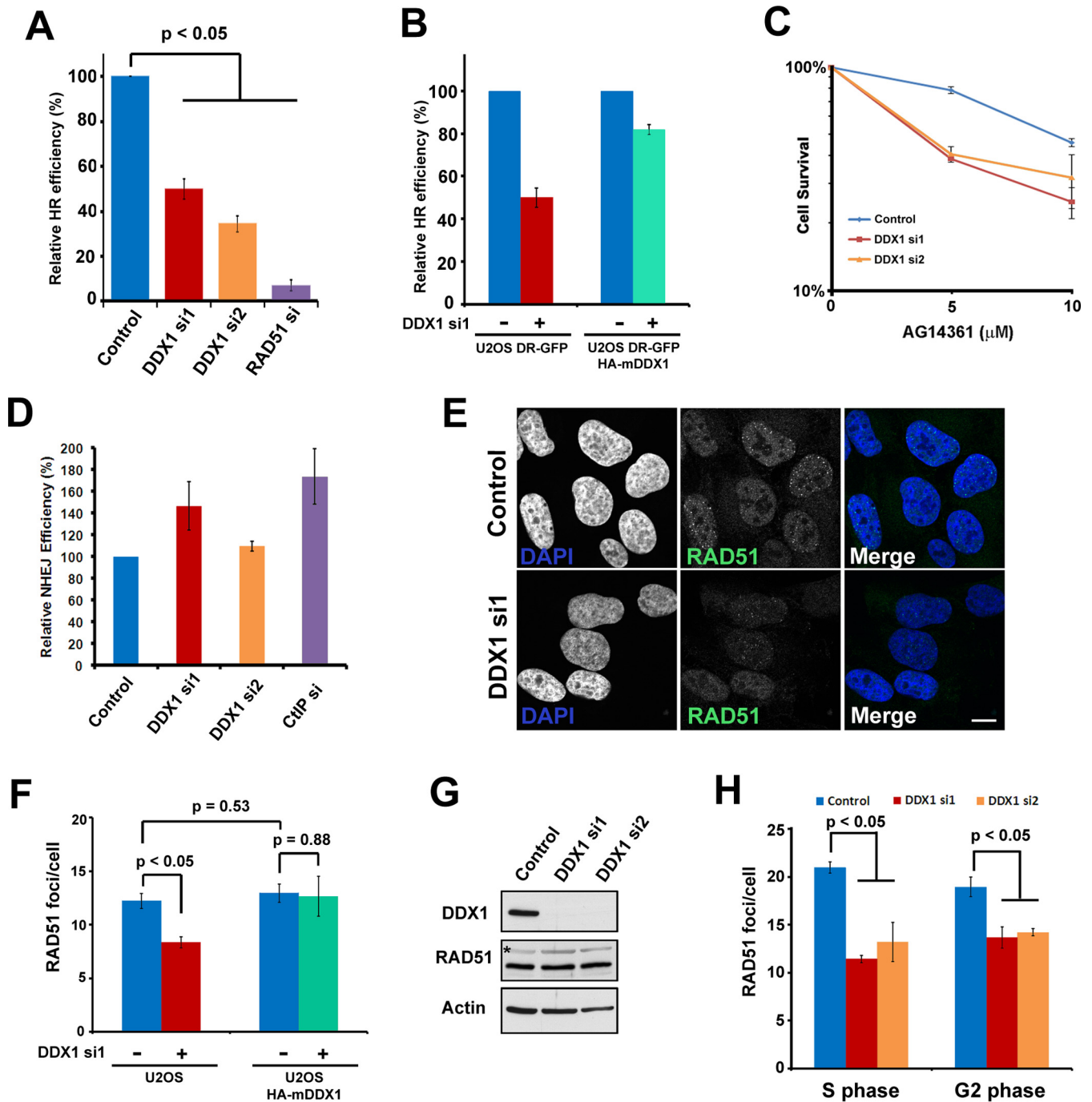


FIG 2 DDX1 facilitates HR-mediated DSB repair. (A) U2OS DR-GFP cells were transfected with scrambled siRNAs (control), DDX1 siRNA (si1 and si2), or RAD51 siRNA. After 72 h, cells were transfected with the same siRNAs along with an I-SceI expression construct by electroporation. GFP-positive cells were analyzed by flow cytometry. Relative HR efficiency was calculated by comparing percentages of GFP-positive cells in DDX1 siRNA- or RAD51 siRNA-treated cells versus control transfectants. (B) U2OS DR-GFP and U2OS DR-GFP HA-mDDX1 cells that stably express siRNA-resistant DDX1 were transfected with scrambled siRNAs (-) or DDX1 (+) siRNA. Relative HR efficiency was measured as described in for panel A. (C) Control and DDX1-depleted U2OS cells were treated with AG14361 at the indicated concentrations for 24 h. Cell survival was measured using the clonogenic assay. (D) Measurement of NHEJ efficiency in control and DDX1-depleted U2OS EJ5-GFP cells. Relative repair efficiency was calculated as described in for panel A. (E) Control and DDX1-depleted U2OS cells were exposed to 3 Gy IR. Cells were immunostained with anti-RAD51 antibody at 2 h post-IR. Bar, 10 μm. (F) U2OS cells and U2OS HA-mDDX1 cells that stably express siRNA-resistant DDX1 were transfected with scrambled (-) or DDX1 (+) siRNA. Numbers of RAD51 foci were analyzed 2 h after 3 Gy IR. For U2OS HA-mDDX1 cells, only cells that express HA-mDDX1 (positive for HA staining) were analyzed. (G) U2OS cells were transfected with scrambled or DDX1 siRNAs. Forty micrograms of lysates was resolved by SDS-PAGE and immunoblotted with the indicated antibodies. Asterisk, residual actin signal. (H) U2OS cells were synchronized using a double thymidine block method. The numbers of RAD51 foci in control and DDX1-depleted cells were analyzed 2 h after 3 Gy treatment in S phase and G₂ phase. For all samples, $n = 3$, except for panel F, where $n = 2$; error bars are SEM. P values were calculated using Fisher's exact test for panels A and H and Student's t test for panel F.

Depletion of DDX1 by two different siRNAs led to reduced RAD51 foci in both S (~40% decrease) and G₂ (~30% decrease) phases (Fig. 2H). The reduction in RAD51 foci is unlikely to be due to direct recruitment of RAD51 by DDX1 since DDX1 does not coimmunoprecipitate with RAD51 (see Fig. S4 in the supplemental material). A possible caveat to this experiment is that RAD51 has been reported to be a common off-target of siRNAs (38). We therefore compared RAD51 protein levels in DDX1-depleted versus control cells. DDX1 knockdown did not affect RAD51 levels, indicating that the reduced number of RAD51 foci observed upon DDX1 depletion is not caused by DDX1 siRNA off-target effects on RAD51. Further evidence against off-target effects comes from DDX1 rescue experiments demonstrating recovery of RAD51 foci in cells transfected with an siRNA-resistant DDX1 expression construct (Fig. 2F).

DDX1 depletion results in decreased ssDNA post-IR. An essential step in the HR repair pathway is generation of ssDNA at the broken DNA ends through extensive end resection. We therefore examined whether DSB-induced ssDNA was affected by DDX1 knockdown in U2OS cells. ssDNA was first analyzed by measuring recruitment of the ssDNA-binding protein RPA following treatment with 5 Gy IR. Compared to control cells, DDX1 knockdown led to fewer RPA foci per cell (~30% reduction) in U2OS but not U2OS HA-mDDX1 cells (Fig. 3B). Upon examination of synchronized U2OS cells in the S and G₂ phases, we observed similar reductions in RPA foci (~30 to 40%) in U2OS cells transfected with either DDX1 si1 or si2 (Fig. 3C).

RPA also forms foci at stalled replication forks in response to replication stress (39). We therefore examined whether the reduced numbers of RPA foci in DDX1-depleted cells could be explained by a possible role for DDX1 in response to replication stress. U2OS cells stably expressing GFP-RPA were treated with 1 mM hydroxyurea (HU) for 1 h to induce stalled replication forks. Similar numbers of GFP-RPA foci were observed in control and DDX1 knockdown cells (see Fig. S5 in the supplemental material), suggesting that the reduced numbers of RPA foci observed upon DDX1 depletion following IR treatment are unlikely to be due to a role for DDX1 in replication. In agreement with this, we have previously shown that DDX1 does not form foci in cells treated with aphidicolin, cisplatin, or UV until 24 h posttreatment, when stalled replication forks eventually collapse and form DSBs (9, 24).

As RPA recruitment measures ssDNA only indirectly, we also used the nondenaturing BrdU staining method (26) to directly visualize ssDNA in control and DDX1-depleted cells. No difference was noted between control and DDX1-depleted cells in the absence of DNA damage, with a nuclear BrdU signal detected in ~2 to 3% of cells. After exposure to 5 Gy IR, ~50% of control cells were positive for nuclear BrdU (Fig. 3D and E). Notably, DDX1 depletion resulted in a significant reduction in the percentage of cells with a nuclear BrdU signal (Fig. 3D and E).

We further analyzed ssDNA in DDX1 knockdown cells using biochemical methods. Phosphorylated RPA (pRPA) and phosphorylated CHK1 (pCHK1) are two commonly used markers for measuring ssDNA generated by end resection (40, 41). First, we examined RPA phosphorylation at Ser 4/Ser 8 upon exposure to 15 Gy, the dose of radiation required to detect RPA phosphorylation by Western blotting (42). RPA phosphorylation was induced in control U2OS cells, with reduced RPA phosphorylation observed in DDX1-depleted cells (Fig. 3F). Similar results were observed for both pRPA and pCHK1 in U2OS cells after exposure to

the radiomimetic drug camptothecin (CPT) (Fig. 3G and H). Taken together, these data indicate that DDX1 either facilitates ssDNA formation or maintains ssDNA at DSBs.

DDX1 is dispensable for efficient end resection at DSBs. ssDNA at DSBs is generated through end resection. End resection at DSBs is a finely orchestrated process which involves multiple players, including nucleases (e.g., MRE11 and EXO1) and stimulation factors (e.g., CtIP). It is generally believed that MRE11 and CtIP initiate resection, whereas EXO1 is required for extensive resection (43). To determine whether DDX1 plays a role in end resection, we first examined the recruitment of CtIP to DSBs in control and DDX1-depleted U2OS cells. As few IR-induced foci were detected upon immunostaining with anti-CtIP antibody, we carried out laser microirradiation (micro-IR) experiments on control and DDX1-depleted U2OS cells. We optimized the micro-IR conditions so that CtIP was recruited only to cells in S and G₂ phases of the cell cycle as determined by cyclin A immunostaining (Fig. 4A), therefore reflecting CtIP's biological role in HR (41). Depletion of DDX1 using either si1 or si2 led to little change in CtIP recruitment to laser tracks in cyclin A-positive cells (Fig. 4B), suggesting that CtIP-dependent resection initiation does not rely on DDX1.

We next examined the extension step of end resection in control and DDX1 knockdown cells. Upon IR, EXO1 rapidly accumulates at DSBs, where it is phosphorylated by ATM following resection initiation and participates in end resection extension (44, 45). Phosphorylation of EXO1 regulates its activity and is required for normal RAD51 focus formation (45). We carried out immunostaining analysis using an antibody that recognizes phosphorylated EXO1 (pEXO1) in DDX1-depleted and control cells subjected to 2 Gy IR. As previously reported (45), pEXO1 formed IR-induced foci in the nucleus (Fig. 4C). In contrast to the reduced number of RAD51 foci observed upon DDX1 knockdown (Fig. 2C), DDX1 depletion had no effect on either the number or the distribution of pEXO1 foci (Fig. 4D) at both 1 h and 3 h post-IR, indicating that DDX1 is dispensable for EXO1-dependent resection extension.

As DDX1 knockdown results in decreased ssDNA at DSBs following IR but has little effect on end resection, we asked whether DDX1 recruitment and/or retention at DSBs resides downstream of end resection. As shown in Fig. 5A, numbers of IR-induced DDX1 foci were significantly reduced upon CtIP depletion. Similar results were also observed in cells depleted of RNF138 (Fig. 5B), an important player in directing DSBs to HR repair and promoting end resection (46, 47). No changes in DDX1 protein levels were detected in either CtIP or RNF138 knockdown cells, indicating a cellular redistribution of DDX1 in these cells (Fig. 5C). Thus, our combined experiments indicate that DDX1 plays a role in the maintenance of the ssDNA rather than in the end resection process itself; however, efficient end resection is critical for DDX1 recruitment/retention at DSBs.

Effects of RNA transcription on DDX1 recruitment and DDX1-mediated HR repair. We have previously shown that pretreatment of HeLa cells with the transcription inhibitor actinomycin D prior to IR exposure abolishes formation of discrete DDX1 foci at DSBs (9). A caveat to this experiment is that actinomycin D has the potential to induce γ -H2AX foci as well as to inhibit transcription (48). To ensure that the effect observed upon actinomycin D treatment is the consequence of transcription inhibition, we tested a second transcription inhibitor, cordycepin, an adenosine

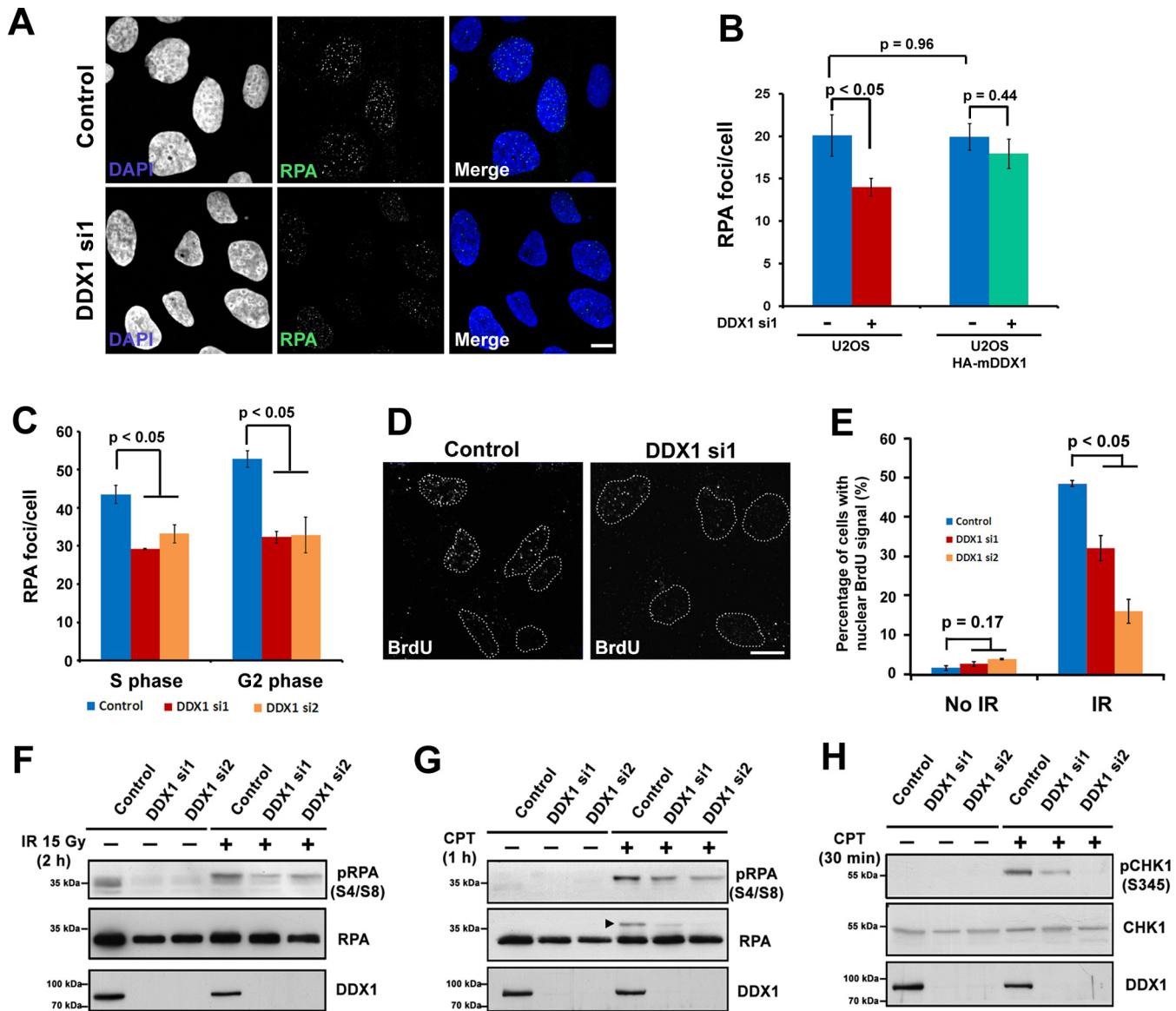


FIG 3 DDX1 depletion results in decreased single-stranded DNA post-IR treatment. (A) U2OS cells were transfected with scrambled siRNA (control) or DDX1 si1. Cells were exposed to 5 Gy IR, extracted, and immunostained with anti-RPA antibody at 2 h post-IR. (B) U2OS and U2OS HA-mDDX1 cells were transfected with scrambled (–) or DDX1 (+) siRNA. RPA foci were analyzed 2 h after 5 Gy IR. For U2OS HA-mDDX1 cells, only cells that express HA-mDDX1 (positive for HA staining) were analyzed. (C) U2OS cells were synchronized using the double thymidine block method. Numbers of RPA foci were analyzed in S phase and G₂ phase of control or DDX1-depleted cells. (D) Control and DDX1-depleted U2OS cells were incubated with 10 μ M BrdU for 24 h and then exposed to 5 Gy IR. Nondenaturing BrdU staining was performed at 3 h post-IR. Note that BrdU also stains mitochondrial DNA in the cytoplasm. The contour of the nuclei is indicated by the dotted lines. (E) Percentages of untreated and IR-treated control and DDX1-depleted cells that are positive for nuclear BrdU. (F) Control and DDX1-depleted U2OS cells were treated with 15 Gy IR and harvested 2 h later. Nuclear extracts were resolved by SDS-PAGE and immunostained with the indicated antibodies. (G and H) Control and DDX1-depleted U2OS cells were treated with 1 μ M CPT for 1 h (G) or 30 min (H). Cells were processed as described above. The arrowhead points to phosphorylated RPA. Scale bars, 10 μ m; error bars, SEM; $n = 3$ for all samples. P values were calculated using the two-sided Student t test (B) or Fisher's exact test (C and E).

analogue that terminates RNA chain elongation (49). Treatment of HeLa cells with cordycepin prior to IR resulted in a significant reduction in IR-induced DDX1 foci (Fig. 6A). Moreover, only 30 to 40% of pretreated cells were positive for IR-induced DDX1 foci, as opposed to 90 to 95% of cells without cordycepin treatment. Similarly, cordycepin pretreatment dramatically impaired DDX1 recruitment to DNA damage sites that were generated by either micro-IR (see Fig. S6 in the supplemental material) or exposure to camptothecin (Fig. 6B). Cordycepin had little effect on γ -H2AX

foci under all tested conditions. Furthermore, DDX1 levels were not affected by cordycepin treatment (Fig. 6C). These combined data indicate that active transcription promotes DDX1 recruitment/retention at DSB sites.

Increased levels of transcripts at DSBs affect DSB repair by HR in DDX1-depleted cells. Given that DDX1 recruitment to DSBs is enhanced by active transcription, we next examined the effect of local transcript deregulation on HR repair in normal and DDX1-depleted U2OS DR-GFP cells. For these experiments, we

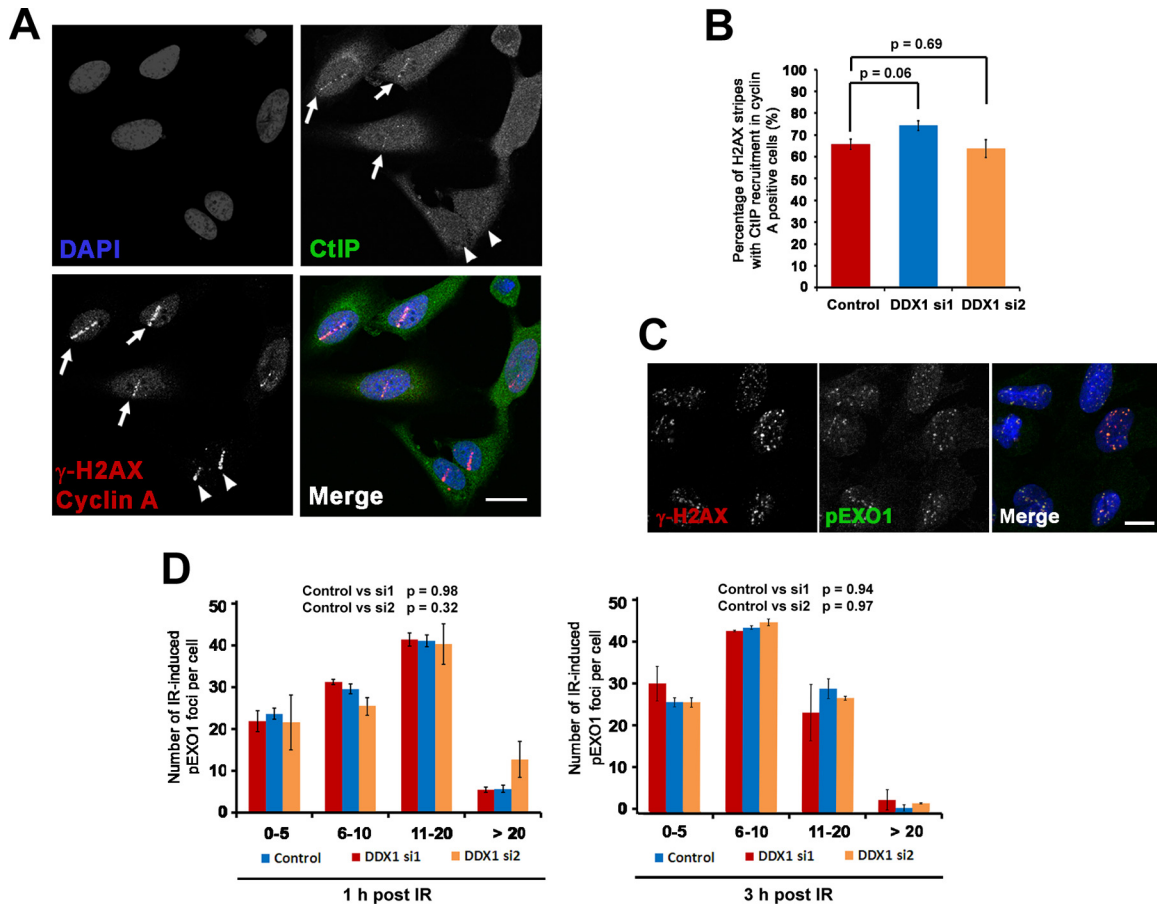


FIG 4 DDX1 depletion has little effect on end resection. (A) Control and DDX1-depleted U2OS cells were microirradiated. Cells were immunostained with anti- γ -H2AX, anti-cyclin A, and anti-CtIP antibodies at 1 h postirradiation. Note that under these conditions, CtIP recruitment occurs in S/G₂-phase cells (indicated by positive nuclear staining of cyclin A, shown by arrows) but not in G₁-phase cells (negative nuclear cyclin A staining, shown by arrowheads). (B) Percentage of γ -H2AX stripes with CtIP recruitment in control and DDX1 knockdown cells treated as described for panel A. (C) Control and DDX1-depleted U2OS cells were treated with 2 Gy IR and immunostained with anti- γ -H2AX and anti-pEXO1 antibodies at 1 h post-IR. (D) Percentage of cells containing pEXO1 foci and number of foci per individual cell at 1 h (left) or 3 h (right) post-IR. *P* values were calculated using the two-sided Student *t* test for panel B and the chi-square test with Yates' correction for panel D. Scale bars, 20 μ m; error bars, SEM; *n* = 3.

used expression constructs containing a 302-bp insert that was complementary to the region immediately upstream of the I-SceI cut site in the DR-GFP locus (Fig. 6D). We chose this 302-bp upstream region for the following reasons. First, we wanted to eliminate the possibility that the construct used to generate the sense or antisense transcripts could itself serve as a homologous sequence template in HR. By using a relatively short sequence that is homologous only to the upstream region of the I-SceI site, we avoided this possible scenario. Second, recent studies have shown that small noncoding RNAs are induced at DSBs (50–52). These small RNAs are transcribed in both orientations and are preferentially generated in the upstream vicinity of DSBs (51, 52).

The 302-bp insert (in either the sense or antisense orientation) was placed downstream of the strong cytomegalovirus (CMV) promoter (to ensure elevated levels of the 302-nt transcripts) and upstream of a polyadenylation signal (to ensure proper termination of the 302-nt transcripts). There was little effect on HR repair (<10% reduction) when U2OS DR-GFP cells were transfected with either the 302-bp sense or antisense construct (Fig. 6E). However, in DDX1-depleted cells, expression of either the sense or antisense 302-nt transcript led to a statistically significant

~30% reduction in HR efficiency (Fig. 6E). These results provide further evidence for RNA involvement in the DDX1-related aspects of DSB repair by HR.

DDX1 does not associate with R-loop-related proteins. We have previously published indirect evidence that DDX1 is recruited to DSBs containing RNA-DNA hybrids (9). The compromised HR efficiency in DDX1-depleted cells in the presence of excessive RNA transcripts complementary to DSBs (Fig. 6E) further implicates RNA-DNA duplexes in DDX1-mediated aspects of DSB repair by HR. R-loops consisting of RNA-DNA duplexes have been implicated in DSB formation and the ensuing cellular response (18–20). We therefore examined whether DDX1 colocalizes with two known markers associated with R-loops: the S9.6 antibody, which specifically recognizes RNA-DNA hybrids (53), and senataxin, an RNA helicase that resolves aberrant R-loops at transcriptionally active chromatin to facilitate proper transcription termination (54). Consistent with previous reports (27, 55), immunostaining with both the S9.6 and antisenataxin antibodies revealed a speckled nuclear pattern without distinct foci (see Fig. S7 and S8 in the supplemental material). Thus, even though purified RNA-DNA hybrids can be immunoprecipitated by the S9.6

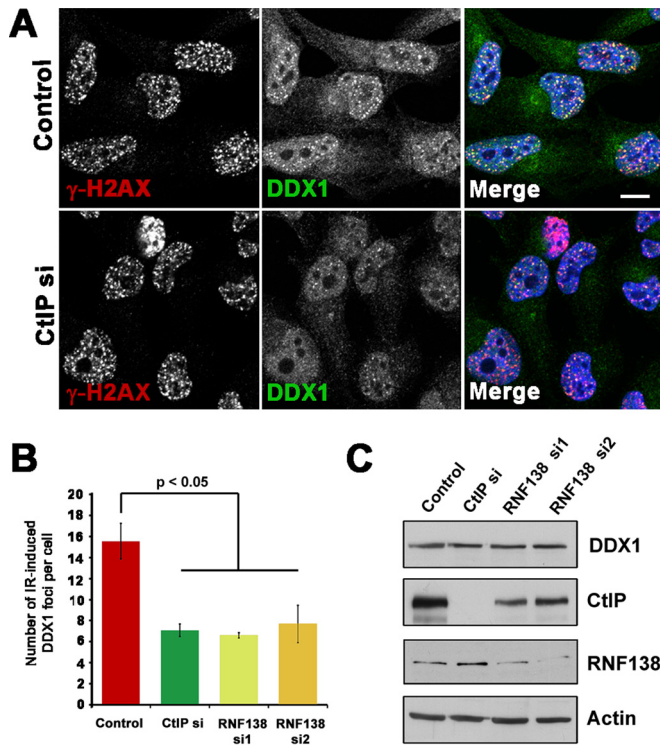


FIG 5 Formation of IR-induced DDX1 foci is dependent on efficient end resection. (A) Control and CtIP-depleted HeLa cells were immunostained with anti- γ -H2AX and anti-DDX1 antibodies at 3 h after treatment with 5 Gy IR. Scale bar, 20 μ m. (B) Cells were treated as described for panel A. The average numbers of IR-induced DDX1 foci in control, CtIP knockdown, or RNF138 knockdown cells were analyzed ($n = 3$). P values were calculated using Fisher's exact test. Error bars, SEM. (C) HeLa cells were transfected with scrambled (control), CtIP, or RNF138 siRNAs. Seventy-two hours later, cells were harvested. Forty micrograms of whole-cell lysates was separated by SDS-PAGE and immunoblotted with the indicated antibodies.

antibody *in vitro* (27, 28), our immunofluorescence data suggest that there is not sufficient accumulation of RNA-DNA duplexes at single sites *in vivo* for detection by immunofluorescence. DDX1 did not coimmunoprecipitate with senataxin after IR treatment (see Fig. S8B), in agreement with the finding that senataxin does not contribute to cell survival post-IR (55).

Overexpression of RNase H has been shown to suppress R-loop formation as well as R-loop-induced phenotypes (17, 18, 29). To address whether RNase H can rescue impaired HR repair in DDX1 knockdown cells, we transfected U2OS DR-GFP cells with an RNase H expression construct along with the plasmid encoding I-SceI nuclease. Overexpression of RNase H had no effect on HR efficiency in both control and DDX1 knockdown cells, indicating that RNase H cannot compensate for DDX1 depletion at DSBs (see Fig. S9 in the supplemental material). Collectively, our data suggest a role for DDX1 in DSB repair that is not related to R-loops.

DDX1 promotes RNA clearance at I-SceI-generated DSBs. To further address RNA-DNA duplex association with DDX1 at DSBs, we carried out DNA-RNA immunoprecipitation (DRIP) analysis using the S9.6 antibody (27, 28). For these experiments, we took advantage of the U2OS DR-GFP/I-SceI system and synchronized DSB formation at the I-SceI site by fusing the I-SceI enzyme to a tamoxifen-responsive hormone-binding domain

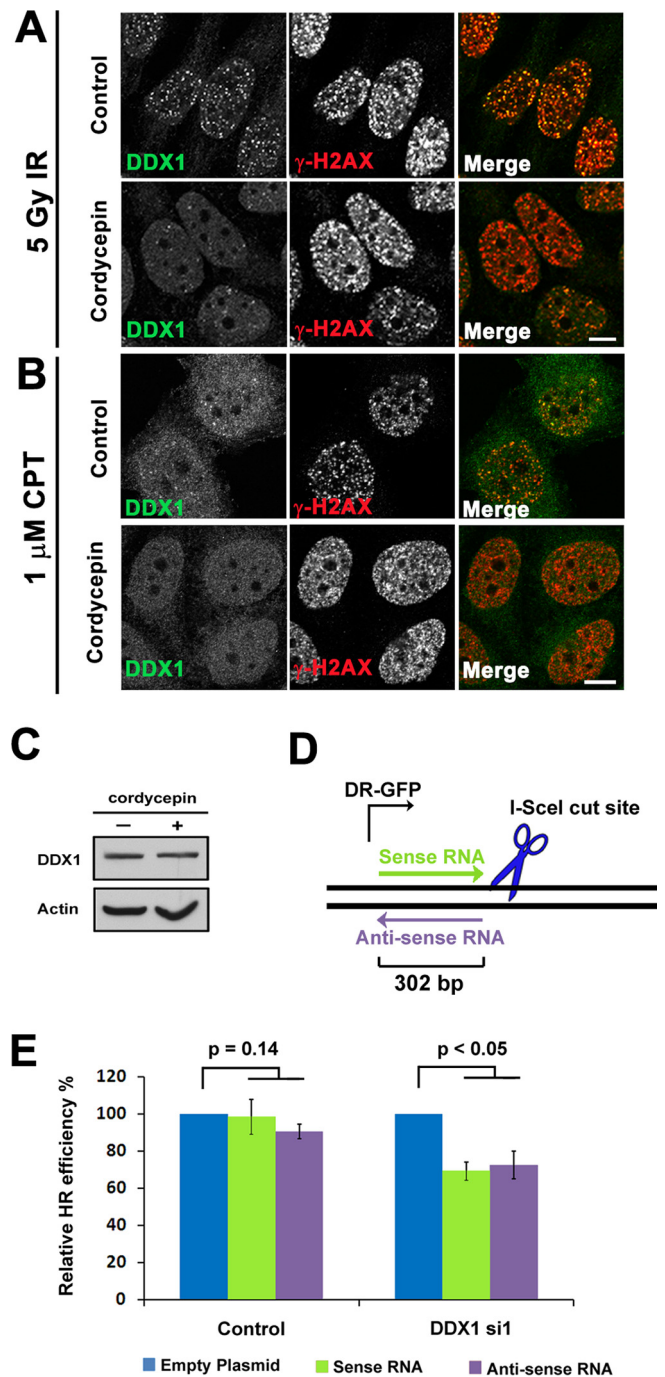


FIG 6 Effects of RNA transcription on DDX1 recruitment/retention at DNA damage sites and DDX1-mediated HR repair. (A) HeLa cells were treated with 100 μ M cordycepin for 2 h (bottom panel) or mock treated (top panel). Cells were then exposed to 5 Gy IR and immunostained at 1 h post-IR. (B) HeLa cells were treated with cordycepin or mock treated as described above. Cells were then incubated with 1 μ M camptothecin for 1 h, followed by immunostaining. Scale bars, 20 μ m. (C) HeLa cells were treated as described for panel B. Forty micrograms of lysates was resolved by SDS-PAGE and immunoblotted with the indicated antibodies. (D) A schematic representation of sense RNA and antisense RNA and their locations relative to the I-SceI cut site in the DR-GFP reporter. The bent arrow indicates the GFP transcription orientation. (E) Empty vector or constructs expressing sense RNA or antisense RNA were transfected into control and DDX1-depleted U2OS DR-GFP cells. Relative HR efficiency was measured as described for Fig. 2A ($n = 3$). Error bars, SEM. P values were calculated using Student's t test.

(ER) and transfecting this fusion construct into U2OS DR-GFP cells. Upon tamoxifen treatment, the ER-I-SceI fusion protein translocates from the cytoplasm to the nucleus and introduces a DSB at the I-SceI site (Fig. 7A). Semiquantitative PCR using primers flanking the I-SceI site was used to assess the efficiency of DSB induction and repair. Based on band intensities in the control and tamoxifen-induced lanes, similar numbers of DSBs were induced and remained unrepaired in control and DDX1 knockdown cells (Fig. 7B). For more quantitative measurements, qPCR was used to amplify the P1 region (Fig. 7A) flanking the I-SceI site. Compared to those in uninduced cells, ~40% of DSBs remained unrepaired in control cells and ~60% in DDX1-depleted cells (Fig. 7C).

Next, we examined whether we could detect RNA-DNA hybrids in the vicinity of the I-SceI site. To do this, we gently extracted nucleic acids containing genomic DNA and associated RNA from control and DDX1-depleted U2OS DR-GFP cells, in which DSBs had been induced at the I-SceI site. Nucleic acids were fragmented by enzyme digestion, followed by immunoprecipitation with the S9.6 antibody. Nucleic acids immunoprecipitated with the S9.6 antibody were then amplified by qPCR. We examined two regions upstream of the I-SceI site, labeled P2 and P3 in Fig. 7A. An approximately 3- to 4-fold increase in qPCR products was observed in DDX1-depleted compared to control U2OS DR-GFP cells at P2 (Fig. 7D) and P3 (Fig. 7E). Pretreatment of the nucleic acid with RNase H prior to adding the S9.6 antibody dramatically reduced the qPCR signal (Fig. 7D and E).

In light of reports indicating that the S9.6 antibody has a low affinity for RNA-RNA hybrids (56) and that pretreatment with RNase A significantly enhances the RNA-DNA signal in DRIP assays (57), we repeated the above-described experiment by pre-treating nucleic acids prepared from tamoxifen-treated U2OS DR-GFP cells with RNase A prior to immunoprecipitation with the S9.6 antibody. Both the P2 and P3 sites were then examined by qPCR. Pretreatment with RNase A led to relative increases of 1.7-fold (P2 site) and 1.3-fold (P3 site) (Fig. 7F), suggesting that the 3- to 4-fold increase in qPCR signal observed in DDX1-depleted cells (Fig. 7D and E) may be an underestimate. Thus, the increased qPCR signal observed upon DDX1 depletion, in conjunction with the decreased qPCR signal observed upon RNase H treatment, indicates a role for DDX1 in the regulation of RNA-DNA hybrids in the vicinity of the I-SceI DSBs.

To confirm that the effect of DDX1 depletion on levels of RNA-DNA hybrids at I-SceI DSBs is indeed due to DDX1 and not to off-target siRNA effects, we carried out DRIP analysis using U2OS DR-GFP HA-mDDX1 cells. Knockdown of endogenous DDX1 in these siRNA-resistant cells failed to increase levels of RNA-DNA duplexes at either the P2 or the P3 site (Fig. 7G), indicating that siRNA-resistant DDX1 protein is able to rescue the increased RNA-DNA duplex phenotype observed upon DDX1 depletion. Collectively, our data indicate that DDX1 plays a key role in resolving DNA-RNA duplexes at I-SceI-induced DSBs.

A novel DSN/RNase H assay to verify clearance of RNA by DDX1 at I-SceI DSBs. To further investigate the role of DDX1 in RNA clearance at DSBs, we designed an assay that uses duplex-specific nuclease (DSN) and RNase H to distinguish DNA-RNA from other nucleic acid structures. DSN specifically degrades DNA from DNA-DNA and DNA-RNA duplexes but has no effect on ssDNA or any form of RNA (58, 59). DSN has been adapted to a variety of applications, including quantitative measurement of ssDNA overhangs in human telomeres (59).

Nucleic acid containing genomic DNA and associated RNA was prepared as described above and treated with DSN alone or pretreated with RNase H followed by DSN (Fig. 8A). The digested nucleic acid was then PCR amplified using primers specific to the I-SceI DSB. Under scenario 1 (no resection and no complementary transcripts), no PCR products will be generated, as DSN will completely digest the double-stranded DNA regardless of RNase H treatment. Under scenario 3 (resection but no complementary transcripts), PCR products will be obtained upon DSN treatment regardless of RNase H treatment, as ssDNA is not digested with either one of these enzymes. Under scenario 2 (resection and the presence of DNA-RNA duplexes), no PCR products will be generated in the presence of DSN alone, as DSN will digest the DNA from both DNA-DNA and DNA-RNA duplexes. However, PCR products will be obtained upon digestion of nucleic acid with RNase H followed by DSN: RNase H will digest RNA from RNA-DNA duplexes, and DSN will digest the double-stranded DNA but not the resulting ssDNA, which can then serve as a template for PCR.

Our DSN/RNase H experiments were carried out using primers that amplify the region immediately upstream of the DSB (Fig. 8A). No PCR products were observed when nucleic acids prepared from cells transfected with either scrambled siRNA or DDX1 siRNA were treated with DSN alone (Fig. 8B, lanes 1 and 3). However, when these same nucleic acids were treated with RNase H followed by DSN, PCR products of the expected size (~320 bp) were generated (Fig. 8B, lanes 2 and 4), indicating the presence of RNA-DNA duplexes upstream of the DSB. Importantly, when DDX1-depleted cells were treated with both RNase H and DSN, there was an increase in PCR products compared to those in control cells (Fig. 8B, compare lanes 4 and 2). Quantitative analysis from multiple experiments ($n = 4$) indicates that the average intensity of PCR products from DDX1-depleted cells is 3- to 4-fold higher than that from control cells (Fig. 8C). These results suggest that depletion of DDX1 results in increased accumulation of RNA-DNA duplexes upstream of I-SceI-induced DSBs. To ensure that DSN digestion was complete under all conditions tested, we used primers specific to the GAPDH gene to carry out PCR amplification using the same nucleic acid templates. No amplified products were observed in any of the DSN/(RNase H)-treated samples (Fig. 8B, lanes 5 to 8). We also used GAPDH primers to confirm that GAPDH could be amplified from untreated nucleic acid samples (Fig. 8B, lane 9). These results indicate that the difference in band intensities observed between lanes 2 and 4 is not due to incomplete DSN digestion.

In control experiments, we tested whether the presence of DNA-RNA duplexes upstream of the I-SceI site was dependent on the formation of DSBs. DSN/RNase H digestion was carried out on nucleic acids extracted from cells transfected with an empty plasmid. In the absence of the I-SceI endonuclease, no DSBs are induced at the I-SceI site, and as a result, the genomic DNA surrounding the I-SceI site should be completely digested by DSN. As expected, neither control nor DDX1-depleted cells generated PCR products after DSN treatment (Fig. 8D). Therefore, the DNA molecules that survived RNase H/DSN digestion and served as the PCR template for Fig. 8B most likely represent RNA-DNA repair intermediates generated as a result of I-SceI-mediated DSB formation.

Taken together, our data from DRIP and DSN/RNase H analyses indicate (i) the presence of RNA-DNA hybrids at the I-SceI-

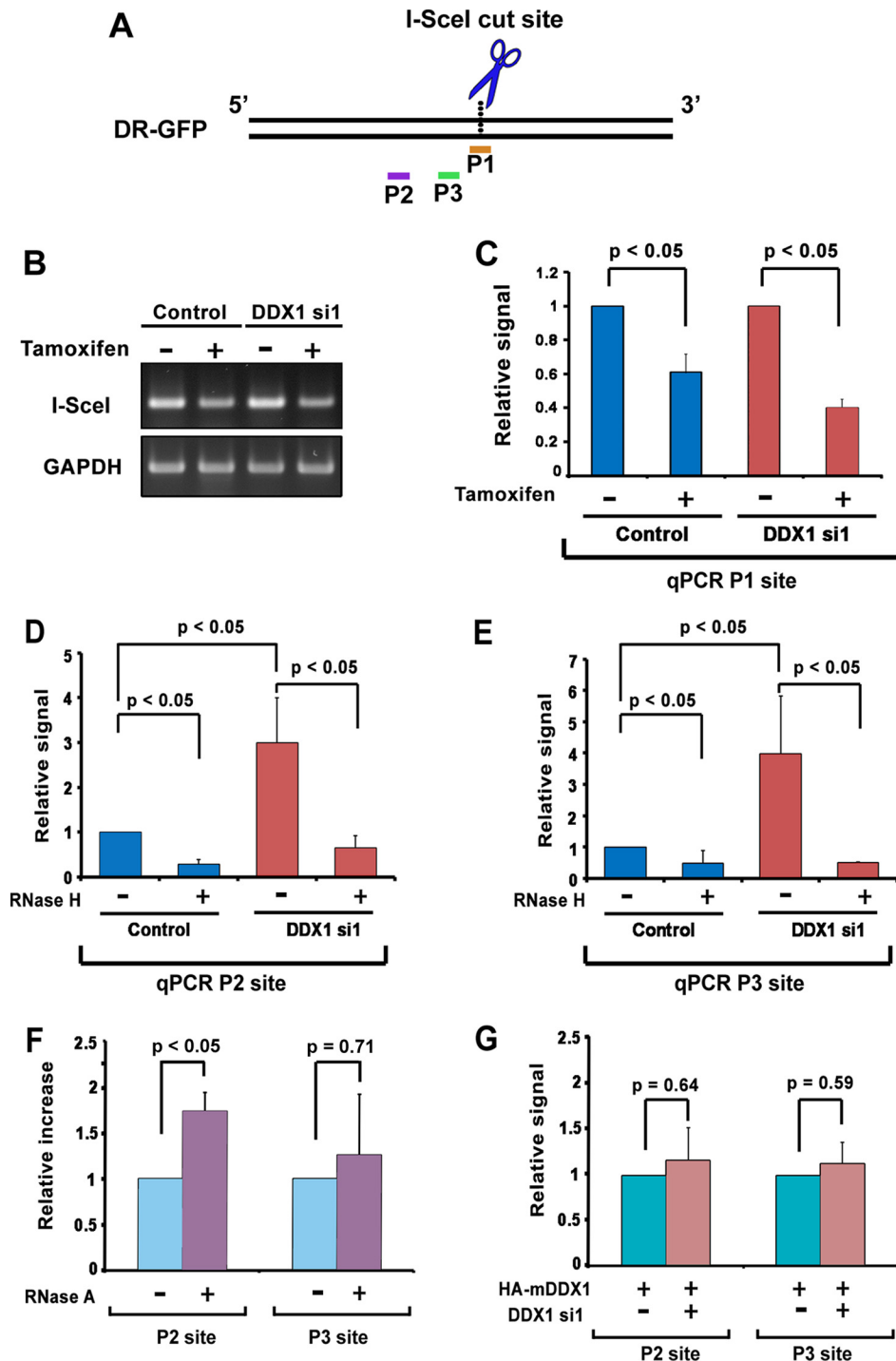


FIG 7 DDX1 promotes clearance of DNA-RNA duplexes formed at the I-SceI-induced DSBs. (A) A schematic illustration showing the position of the I-SceI-induced DSB in the DR-GFP reporter and the three sites (P1 to P3) targeted for analysis by qPCR. (B) U2OS DR-GFP cells were transfected with scrambled siRNA (control) or DDX1 siRNA (DDX1 si1). Cells were then transfected with the HA-ER-I-SceI construct, and DSBs at the I-SceI site were induced with 5 μ M tamoxifen for 4 h. Genomic DNA (50 ng) was amplified by semiquantitative PCR with primers flanking the I-SceI cut site (labeled P1 in panel A) (upper panel) or GAPDH-specific primers (bottom panel). (C) qPCR analysis of the region spanning the I-SceI cut site (P1 site) in cells described for panel B. Signal intensities were normalized against a GAPDH control. (D and E) DRIP analysis was carried out using the S9.6 antibody and nucleic acid purified from control (scrambled siRNA-transfected) and DDX1-depleted U2OS DR-GFP cells with DSBs induced at I-SceI sites. qPCR was performed using primers specific to sites P2 (D) and P3 (E). Where indicated, samples were treated with RNase H prior to DRIP analysis. Signal intensities were normalized against input DNA as well as the SNRPN negative control. (F) DRIP-qPCR analysis was performed as described above. Where indicated, samples were treated with RNase A prior to DRIP. Relative increases in the qPCR signal were calculated by comparing the ratio of the qPCR signal in DDX1-depleted versus control cells treated with RNase A with the ratio of the qPCR signal in DDX1-depleted control cells without RNase A treatment. (G) U2OS DR-GFP cells stably expressing HA-mDDX1 were transfected with scrambled siRNA (-) or DDX1 si1 (+). DRIP-qPCR analysis was performed as described for panels D and E. *P* values were calculated using the Mann-Whitney test; *n* = 3 for all cases.

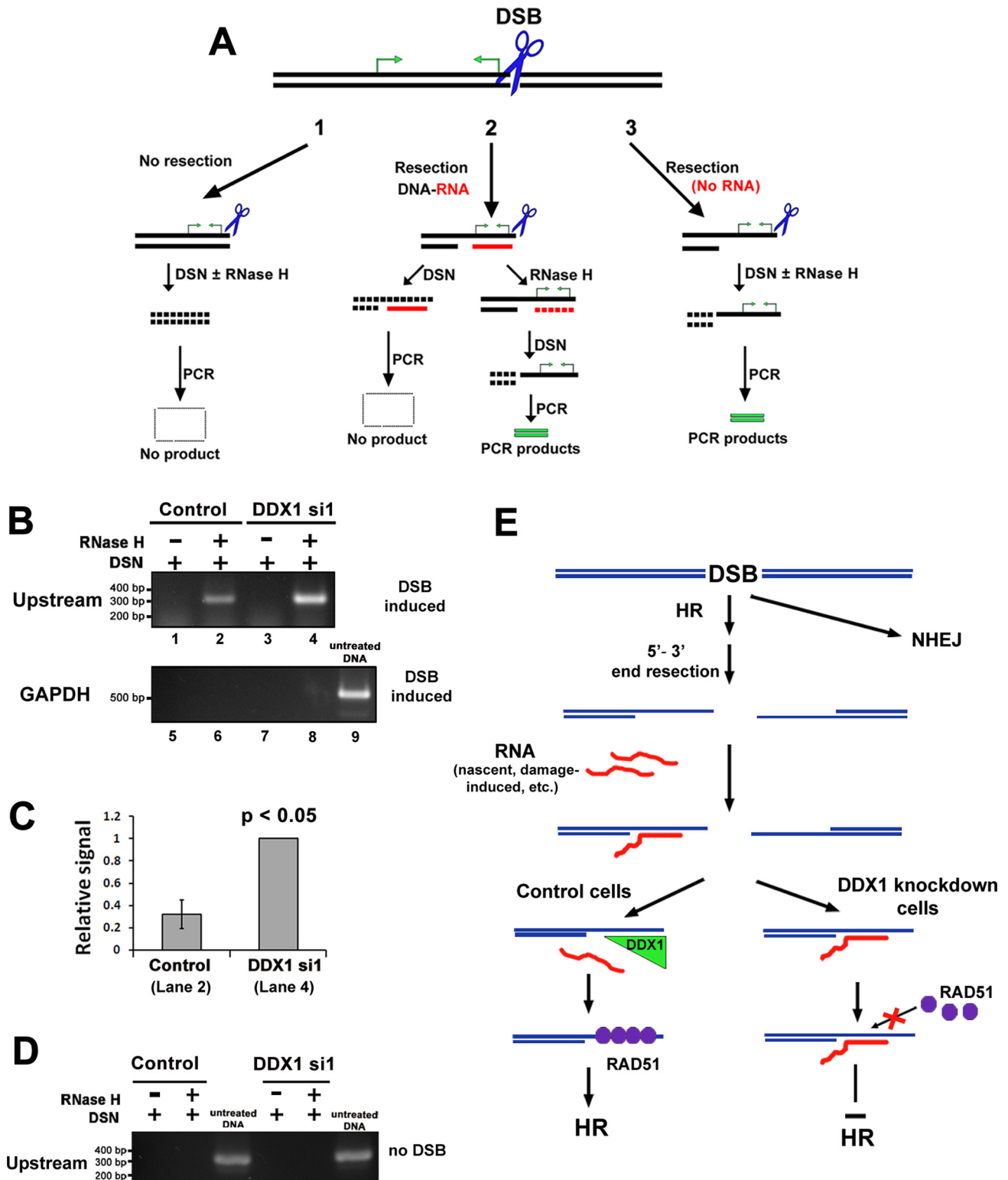


FIG 8 DDX1 promotes RNA clearance at I-SceI-induced DSBs. (A) Three possible scenarios at I-SceI-induced DSBs. The positions of primers (upstream region) are indicated by the green arrows. Note that RNA molecules can be either long and continuous (as shown) or short and discontinuous. (B) DSBs at I-SceI sites were induced by tamoxifen in control or DDX1-depleted U2OS DR-GFP cells. One microgram of nucleic acid was digested with DSN alone or RNase H followed by DSN. Digested DNA (250 ng) was PCR amplified using primers specific to the upstream region of the I-SceI cut site (lanes 1 to 4) or GAPDH primers (lanes 5 to 8). For comparison, 50 ng of intact DNA from control cells (transfected with scrambled siRNA and ER-I-SceI expression vector and induced by tamoxifen) was PCR amplified using GAPDH primers (lane 9). (C) Average intensity of PCR products in panel B from four independent experiments. The *P* value was calculated using Student's *t* test. (D) Control or DDX1-depleted U2OS DR-GFP cells were transfected with an ER expression construct, followed by tamoxifen induction. PCR was performed as described for panel B. (E) Model of the proposed role for DDX1 in HR. See the text for details.

induced DSB and (ii) a role for DDX1 in clearing RNA from ssDNAs generated at the DSB sites.

DISCUSSION

Impressive advances have been made in our understanding of the proteins and pathways involved in the repair of DSBs by error-prone NHEJ and error-free HR. Recent data suggest a role for RNA in the repair of at least a subset of DSBs. However, we still do not know whether the presence of RNA affects pathway choice and/or repair efficiency. DDX1 is a member of the RNA helicase family of DEAD box proteins that has both RNA-RNA and RNA-DNA unwinding activities (9). DDX1 has previously been implicated in the cellular response to DNA DSBs based on its (i) recruitment to a subset of DSBs after exposure of cells to IR, (ii) ATM-dependent and IR-induced phosphorylation, and (iii) interaction with ATM and the MRN complex (9). Importantly, treatment of irradiated cells with either RNase H or actinomycin D reveals a role for RNA-DNA duplex structures or transcription, respectively, in either the recruitment or retention of DDX1 at DSBs (9). These combined data suggest the intriguing possibility that DDX1 is involved in the repair of DSBs at sites of active transcription. Here, we show that DDX1 is required for efficient repair of DSBs by HR, with a specific role in the maintenance of ssDNA generated through the end resection step of DSB repair by HR. We used a combination of assays, including a novel DSN/RNase H assay, to directly demonstrate the presence of RNA-DNA duplexes in the vicinity of DSBs and the retention of RNA-DNA duplexes at DSBs in DDX1-depleted cells. Our results indicate a role for DDX1 in facilitating HR repair by either unwinding or remodelling RNA-DNA duplex structures that are formed once the ssDNA has been generated by end resection.

DDX1 maintains ssDNA and facilitates HR. There is accumulating evidence for the involvement of RNA-binding proteins in DSB repair (60). For example, Polo et al. (61) reported that hnRNP U-like proteins, hnRNPUL1 and -2, positively regulate end resection at DSBs and promote repair via the HR pathway. In a genome-wide screen designed to identify the players in HR, RBMX was found to facilitate BRCA2 expression and promote HR (38). From the same screen, another DEAD box protein, DDX17, was shown to accumulate at micro-IR-induced damage sites and to suppress HR-mediated repair through unknown mechanisms.

By analyzing various steps of HR repair, we found that DDX1 depletion results in reduced numbers of RPA, BrdU, and RAD51 foci, as well as defective phosphorylation of RPA and CHK1, in cells treated with IR. As these assays are commonly used for measuring ssDNA formation, our results suggest that DDX1 knock-down specifically affects the ssDNA produced as the result of end resection following DSB formation. Intriguingly, when we analyzed end resection, the step in HR that generates ssDNA, we observed normal recruitment of CtIP and phosphorylation of EXO1 at DSBs in DDX1-depleted cells, suggesting that DDX1 is not essential for end resection. Moreover, DDX1 accumulation at DSBs is dependent on efficient end resection, thereby placing DDX1 focus formation downstream of end resection. These combined data point to a role for DDX1 in the maintenance of ssDNA once it is generated by end resection. While the ssDNA-binding protein RPA has a well-established role in stabilizing ssDNA (62), other proteins or factors may also be involved in this process. For example, RNAs complementary to ssDNAs may interfere with processes downstream of end resection in HR unless they are removed

by DDX1. In agreement with its role in maintaining ssDNA, DDX1 has been shown to interact with ssDNA coated with RPA (63).

DDX1 resolves RNA-containing duplex structures at DSBs. The RNA-DNA structures resolved at DSBs by DDX1 are reminiscent of R-loops, first described at transcriptionally active sites of the genome (13–15). R-loops are three-stranded nucleic acid structures consisting of a DNA-RNA hybrid associated with the genomic ssDNA template. A growing body of evidence suggests that cotranscriptional R-loops contribute to DSB formation, possibly due to collisions between the replication and transcription machineries at the unresolved R-loops (13–15). In addition, R-loops as detected by RNase H recruitment have also been observed at micro-IR-induced DNA lesions immediately following DNA damage (20).

We used a number of approaches to investigate possible similarities between traditionally defined R-loops and the RNA-DNA structures that we identified at DSBs. First, DNA replication stress, shown by others to induce R-loop formation (64, 65), did not result in accumulation of DDX1 at chromatin (9, 24). However, DDX1 foci were observed 24 h after replication disruption, when stalled replication forks eventually collapse and form DSBs. Second, although others have shown that R-loops and R-loop-induced phenotypes can be suppressed by overexpression of RNase H (17, 18, 54), RNase H overexpression did not compensate for DDX1 depletion as measured by the DR-GFP reporter assay. Third, recruitment of RNase H and other R-loop-associated factors to DNA lesions induced by micro-IR is rapid but transient (recruitment occurs within minutes, with factors then dissociating from the DNA lesions) (20), whereas DDX1 accumulation at DSBs follows much slower kinetics (peaks at 1 h, with no dissociation detected for hours), suggesting that RNase H and DDX1 either play different roles or act at different stages in resolving RNA-DNA structures during the DSB repair process. Fourth, senataxin, an RNA helicase that plays a critical role in resolving R-loops *in vivo* (54, 64), did not coimmunoprecipitate with DDX1 in either the presence or absence of IR-induced DNA damage. Although we cannot eliminate the possibility that RNase H access to DSBs was blocked by proteins recruited to these sites, our combined results are consistent with DDX1-resolved RNA-DNA hybrids being different from R-loops. Thus, DDX1, RNase H, and senataxin may all play different roles in resolving RNA-DNA hybrids, depending on the context.

A number of studies have shown that RNA species, especially noncoding RNAs (ncRNAs), are important players in the cellular response following DSB formation (66, 67). For example, DSBs induce biogenesis of microRNAs, which in turn modulate the DNA repair process by regulating the expression of ATM and RAD52 (68). These microRNAs are not generated at DSB sites, nor do they have sequence homology to DNA regions flanking DSBs. Recently, a new category of small ncRNAs associated with DSBs has been discovered. These small ncRNAs are called DSB-induced small RNAs (diRNA) or DNA damage-induced RNAs (DDRNA) because they are induced in the vicinity of DSBs (50, 51). diRNAs are transcribed from both DNA strands. Biogenesis of diRNAs requires key players in the RNA interference pathway, such as Dicer and Drosha. Interestingly, inhibition of diRNA generation appears to reduce only HR efficiency and not NHEJ in mammalian cells (69). How diRNA functions at DNA lesions remains to be elucidated.

Using two assays, DRIP and DSN/RNase H, we demonstrated the presence of RNA-DNA duplexes in the vicinity of I-SceI-generated DSBs. Based on high-throughput sequencing, diRNAs are complementary to both strands of DNA in the vicinity of DSBs and can be found within a few kilobases both upstream and downstream of DSBs (51). Thus, the source of the RNA in the RNA-DNA hybrids could be diRNAs but could also be alternative RNA species such as mRNAs (or fragments thereof), since our assay does not discriminate between short, discontinuous RNAs and longer, more continuous molecules.

Attempts to determine whether a gene's transcriptional activity affects the pathway by which DSBs will be repaired have produced conflicting results. For example, no correlation was found between transcription activity and HR repair using a GFP-based reporter assay (21). In contrast, by examining multiple endogenous cut sites, Aymard et al. found a significant increase in HR when DSBs were located in euchromatic regions and/or next to actively transcribed genes (70). Similar results were also reported by Gong et al. (71). While our study does not directly address repair pathway choice for DSBs, we do show an association between DDX1 and efficient repair by HR that is linked to transcription and the presence of RNA at DSBs. We propose the following model for the role of DDX1 at DSBs (Fig. 8E). Upon DSB formation, for those lesions that are channeled to HR, end resection is activated, generating ssDNA. If DSBs are in the vicinity of active transcription, RNA may anneal to the complementary ssDNA, thus impeding the later steps in HR (e.g., RAD51 nucleofilament formation on ssDNA). DDX1 is recruited to DSB sites in an ATM-dependent manner, where it unwinds RNA-DNA duplexes, exposes the ssDNA, and facilitates downstream events such as RAD51 nucleofilament formation. In DDX1 knockdown cells, the RNA-DNA structures persist and impede efficient HR.

Of note, in addition to HR repair, DDX1 knockdown also impairs DSB repair in G₁ phase when canonical HR is suppressed, suggesting that DDX1 may contribute to other types of DSB repair. In agreement with this idea, IR-induced DDX1 foci are found throughout the cell cycle (9). Based on our data, DDX1 knockdown has only a subtle effect on NHEJ; the DSB repair pathway believed to repair most DSBs prior to DNA replication. However, recent evidence suggests that novel DSB repair pathways involving RNA templates may be functional throughout the cell cycle, including G₁. RNA template-guided DSB repair has been reported in both mammalian cells and bacteria and involves RNA molecules that serve as templates to guide DNA synthesis during DSB repair (72–76). Regulation of RNA-DNA duplexes, including both their formation and resolution, may be critical to this repair process. As DEAD box proteins have been implicated in both the formation and resolution of RNA-RNA duplexes (77, 78), we speculate that DDX1, with its ability to unwind either RNA-RNA or RNA-DNA duplexes, could play a fundamental role in RNA template-guided DSB repair.

In conclusion, we demonstrate a role for DDX1 in the repair of DSBs by HR through maintenance of the ssDNA generated by end resection. By examining DNA-RNA duplex structures at DSBs, we showed that DDX1 clears RNA from RNA-DNA duplexes located in the vicinity of DSBs that are marked for repair by HR. Thus, our data functionally implicate a member of the DEAD box family of RNA helicases in DSB repair and indicate that RNA, in addition to RPA proteins, can regulate the availability of ssDNA for the subsequent steps in HR.

ACKNOWLEDGMENTS

This work was supported by operating grants from the Alberta Cancer Foundation and Canadian Breast Cancer Foundation. D.R.G. is a recipient of an Alberta Innovates-Health Solutions graduate studentship.

We thank Maria Jasin, Jeremy Stark, Ranjit Bindra, Stephen Leppla, Bradley Carins, Martin Lavin, Kum Kum Khanna, Gordon Chan, and Ajit Sharma for their kind donations of cell lines and antibodies. We are indebted to Ismail Ismail and Sachin Katyal for helpful comments and sharing unpublished data. We thank Frederic Chedin for sharing the DRIP protocol. We are grateful to Xuejun Sun and Gerry Barron for help with the Imaris software.

None of the authors involved in the preparation of the manuscript have any conflicts of interest to report.

FUNDING INFORMATION

The Alberta Cancer Foundation (grant number 25033) and the Canadian Breast Cancer Foundation provided funding to Roseline Godbout. The Alberta Innovates Health Solutions provided stipend funding to Devon R. Germain.

REFERENCES

1. Godbout R, Li L, Liu RZ, Roy K. 2007. Role of DEAD box 1 in retinoblastoma and neuroblastoma. *Future Oncol* 3:575–587. <http://dx.doi.org/10.2217/14796694.3.5.575>.
2. Germain DR, Graham K, Glubrecht DD, Hugh JC, Mackey JR, Godbout R. 2011. DEAD box 1: a novel and independent prognostic marker for early recurrence in breast cancer. *Breast Cancer Res Treat* 127:53–63. <http://dx.doi.org/10.1007/s10549-010-0943-7>.
3. Germain DR, Li L, Hildebrandt MR, Simmonds AJ, Hughes SC, Godbout R. 2015. Loss of the *Drosophila melanogaster* DEAD box protein Ddx1 leads to reduced size and aberrant gametogenesis. *Dev Biol* 407:232–245. <http://dx.doi.org/10.1016/j.ydbio.2015.09.012>.
4. Hildebrandt MR, Germain DR, Monckton EA, Brun M, Godbout R. 2015. Ddx1 knockout results in transgenerational wild-type lethality in mice. *Sci Rep* 5:9829. <http://dx.doi.org/10.1038/srep09829>.
5. Chou CF, Lin WJ, Lin CC, Lubner CA, Godbout R, Mann M, Chen CY. 2013. DEAD box protein DDX1 regulates cytoplasmic localization of KSRP. *PLoS One* 8:e73752. <http://dx.doi.org/10.1371/journal.pone.0073752>.
6. Kanai Y, Dohmae N, Hirokawa N. 2004. Kinesin transports RNA: isolation and characterization of an RNA-transporting granule. *Neuron* 43:513–525. <http://dx.doi.org/10.1016/j.neuron.2004.07.022>.
7. Vessey JP, Amadei G, Burns SE, Kiebler MA, Kaplan DR, Miller FD. 2012. An asymmetrically localized staufen2-dependent RNA complex regulates maintenance of mammalian neural stem cells. *Cell Stem Cell* 11:517–528. <http://dx.doi.org/10.1016/j.stem.2012.06.010>.
8. Popow J, Jurkin J, Schleiffer A, Martinez J. 2014. Analysis of orthologous groups reveals archease and DDX1 as tRNA splicing factors. *Nature* 511:104–107. <http://dx.doi.org/10.1038/nature13284>.
9. Li L, Monckton EA, Godbout R. 2008. A role for DEAD box 1 at DNA double-strand breaks. *Mol Cell Biol* 28:6413–6425. <http://dx.doi.org/10.1128/MCB.01053-08>.
10. Ciccio A, Elledge SJ. 2010. The DNA damage response: making it safe to play with knives. *Mol Cell* 40:179–204. <http://dx.doi.org/10.1016/j.molcel.2010.09.019>.
11. Polo SE, Jackson SP. 2011. Dynamics of DNA damage response proteins at DNA breaks: a focus on protein modifications. *Genes Dev* 25:409–433. <http://dx.doi.org/10.1101/gad.2021311>.
12. Han C, Liu Y, Wan G, Choi HJ, Zhao L, Ivan C, He X, Sood AK, Zhang X, Lu X. 2014. The RNA-binding protein DDX1 promotes primary microRNA maturation and inhibits ovarian tumor progression. *Cell Rep* 8:1447–1460. <http://dx.doi.org/10.1016/j.celrep.2014.07.058>.
13. Hamperl S, Cimprich KA. 2014. The contribution of co-transcriptional RNA:DNA hybrid structures to DNA damage and genome instability. *DNA Repair (Amst)* 19:84–94. <http://dx.doi.org/10.1016/j.dnarep.2014.03.023>.
14. Aguilera A, Garcia-Muse T. 2012. R loops: from transcription byproducts to threats to genome stability. *Mol Cell* 46:115–124. <http://dx.doi.org/10.1016/j.molcel.2012.04.009>.
15. Skourti-Stathaki K, Proudfoot NJ. 2014. A double-edged sword: R loops

- as threats to genome integrity and powerful regulators of gene expression. *Genes Dev* 28:1384–1396. <http://dx.doi.org/10.1101/gad.242990.114>.
16. Huertas P, Aguilera A. 2003. Cotranscriptionally formed DNA:RNA hybrids mediate transcription elongation impairment and transcription-associated recombination. *Mol Cell* 12:711–721. <http://dx.doi.org/10.1016/j.molcel.2003.08.010>.
 17. Li X, Manley JL. 2005. Inactivation of the SR protein splicing factor ASF/SF2 results in genomic instability. *Cell* 122:365–378. <http://dx.doi.org/10.1016/j.cell.2005.06.008>.
 18. Paulsen RD, Soni DV, Wollman R, Hahn AT, Yee MC, Guan A, Hesley JA, Miller SC, Cromwell EF, Solow-Cordero DE, Meyer T, Cimprich KA. 2009. A genome-wide siRNA screen reveals diverse cellular processes and pathways that mediate genome stability. *Mol Cell* 35:228–239. <http://dx.doi.org/10.1016/j.molcel.2009.06.021>.
 19. Stirling PC, Chan YA, Minaker SW, Aristizabal MJ, Barrett I, Sipahimalani P, Kobor MS, Hieter P. 2012. R-loop-mediated genome instability in mRNA cleavage and polyadenylation mutants. *Genes Dev* 26:163–175. <http://dx.doi.org/10.1101/gad.179721.111>.
 20. Britton S, Dernoncourt E, Deltell C, Froment C, Schiltz O, Salles B, Frit P, Calsou P. 2014. DNA damage triggers SAF-A and RNA biogenesis factors exclusion from chromatin coupled to R-loops removal. *Nucleic Acids Res* 42:9047–9062. <http://dx.doi.org/10.1093/nar/gku601>.
 21. Gunn A, Bennardo N, Cheng A, Stark JM. 2011. Correct end use during end joining of multiple chromosomal double strand breaks is influenced by repair protein RAD50, DNA-dependent protein kinase DNA-PKcs, and transcription context. *J Biol Chem* 286:42470–42482. <http://dx.doi.org/10.1074/jbc.M111.309252>.
 22. Xia B, Sheng Q, Nakanishi K, Ohashi A, Wu J, Christ N, Liu X, Jasin M, Couch FJ, Livingston DM. 2006. Control of BRCA2 cellular and clinical functions by a nuclear partner, PALB2. *Mol Cell* 22:719–729. <http://dx.doi.org/10.1016/j.molcel.2006.05.022>.
 23. Weinstock DM, Nakanishi K, Helgadottir HR, Jasin M. 2006. Assaying double-strand break repair pathway choice in mammalian cells using a targeted endonuclease or the RAG recombinase. *Methods Enzymol* 409:524–540. [http://dx.doi.org/10.1016/S0076-6879\(05\)09031-2](http://dx.doi.org/10.1016/S0076-6879(05)09031-2).
 24. Li L, Roy K, Katyal S, Sun X, Bleoo S, Godbout R. 2006. Dynamic nature of cleavage bodies and their spatial relationship to DDX1 bodies, Cajal bodies, and gems. *Mol Biol Cell* 17:1126–1140.
 25. Bleoo S, Sun X, Hendzel MJ, Rowe JM, Packer M, Godbout R. 2001. Association of human DEAD box protein DDX1 with a cleavage stimulation factor involved in 3'-end processing of pre-mRNA. *Mol Biol Cell* 12:3046–3059. <http://dx.doi.org/10.1091/mbc.12.10.3046>.
 26. Buonomo SB, Wu Y, Ferguson D, de Lange T. 2009. Mammalian Rif1 contributes to replication stress survival and homology-directed repair. *J Cell Biol* 187:385–398. <http://dx.doi.org/10.1083/jcb.200902039>.
 27. Bhatia V, Barroso SI, Garcia-Rubio ML, Tumini E, Herrera-Moyano E, Aguilera A. 2014. BRCA2 prevents R-loop accumulation and associates with TREX-2 mRNA export factor PCID2. *Nature* 511:362–365. <http://dx.doi.org/10.1038/nature13374>.
 28. Ginno PA, Lott PL, Christensen HC, Korf I, Chedin F. 2012. R-loop formation is a distinctive characteristic of unmethylated human CpG island promoters. *Mol Cell* 45:814–825. <http://dx.doi.org/10.1016/j.molcel.2012.01.017>.
 29. Herrera-Moyano E, Mergui X, Garcia-Rubio ML, Barroso S, Aguilera A. 2014. The yeast and human FACT chromatin-reorganizing complexes solve R-loop-mediated transcription-replication conflicts. *Genes Dev* 28:735–748. <http://dx.doi.org/10.1101/gad.234070.113>.
 30. Lobrich M, Shibata A, Beucher A, Fisher A, Ensminger M, Goodarzi AA, Barton O, Jeggo PA. 2010. γ H2AX foci analysis for monitoring DNA double-strand break repair: strengths, limitations and optimization. *Cell Cycle* 9:662–669. <http://dx.doi.org/10.4161/cc.9.4.10764>.
 31. Beucher A, Birraux J, Tchouandong L, Barton O, Shibata A, Conrad S, Goodarzi AA, Krempler A, Jeggo PA, Lobrich M. 2009. ATM and Artemis promote homologous recombination of radiation-induced DNA double-strand breaks in G2. *EMBO J* 28:3413–3427. <http://dx.doi.org/10.1038/emboj.2009.276>.
 32. Bee L, Fabris S, Cherubini R, Mognato M, Celotti L. 2013. The efficiency of homologous recombination and non-homologous end joining systems in repairing double-strand breaks during cell cycle progression. *PLoS One* 8:e69061. <http://dx.doi.org/10.1371/journal.pone.0069061>.
 33. Rothkamm K, Kruger I, Thompson LH, Lobrich M. 2003. Pathways of DNA double-strand break repair during the mammalian cell cycle. *Mol Cell Biol* 23:5706–5715. <http://dx.doi.org/10.1128/MCB.23.16.5706-5715.2003>.
 34. Alagoz M, Katsuki Y, Ogiwara H, Ogi T, Shibata A, Kakarougkas A, Jeggo P. 2015. SETDB1, HP1 and SUV39 promote repositioning of 53BP1 to extend resection during homologous recombination in G2 cells. *Nucleic Acids Res* 43:7931–7944. <http://dx.doi.org/10.1093/nar/gkv722>.
 35. Bryant HE, Schultz N, Thomas HD, Parker KM, Flower D, Lopez E, Kyle S, Meuth M, Curtin NJ, Helleday T. 2005. Specific killing of BRCA2-deficient tumours with inhibitors of poly(ADP-ribose) polymerase. *Nature* 434:913–917. <http://dx.doi.org/10.1038/nature03443>.
 36. Farmer H, McCabe N, Lord CJ, Tutt AN, Johnson DA, Richardson TB, Santarosa M, Dillon KJ, Hickson I, Knights C, Martin NM, Jackson SP, Smith GC, Ashworth A. 2005. Targeting the DNA repair defect in BRCA mutant cells as a therapeutic strategy. *Nature* 434:917–921. <http://dx.doi.org/10.1038/nature03445>.
 37. Krejci L, Altmannova V, Spirek M, Zhao X. 2012. Homologous recombination and its regulation. *Nucleic Acids Res* 40:5795–5818. <http://dx.doi.org/10.1093/nar/gks270>.
 38. Adamson B, Smogorzewska A, Sigoillot FD, King RW, Elledge SJ. 2012. A genome-wide homologous recombination screen identifies the RNA-binding protein RBMX as a component of the DNA-damage response. *Nat Cell Biol* 14:318–328. <http://dx.doi.org/10.1038/ncb2426>.
 39. Vassin VM, Wold MS, Borowiec JA. 2004. Replication protein A (RPA) phosphorylation prevents RPA association with replication centers. *Mol Cell Biol* 24:1930–1943. <http://dx.doi.org/10.1128/MCB.24.5.1930-1943.2004>.
 40. MacDougall CA, Byun TS, Van C, Yee MC, Cimprich KA. 2007. The structural determinants of checkpoint activation. *Genes Dev* 21:898–903. <http://dx.doi.org/10.1101/gad.1522607>.
 41. Sartori AA, Lukas C, Coates J, Mistrik M, Fu S, Bartek J, Baer R, Lukas J, Jackson SP. 2007. Human CtIP promotes DNA end resection. *Nature* 450:509–514. <http://dx.doi.org/10.1038/nature06337>.
 42. Shao RG, Cao CX, Zhang H, Kohn KW, Wold MS, Pommier Y. 1999. Replication-mediated DNA damage by camptothecin induces phosphorylation of RPA by DNA-dependent protein kinase and dissociates RPA: DNA-PK complexes. *EMBO J* 18:1397–1406. <http://dx.doi.org/10.1093/emboj/18.5.1397>.
 43. Symington LS, Gautier J. 2011. Double-strand break end resection and repair pathway choice. *Annu Rev Genet* 45:247–271. <http://dx.doi.org/10.1146/annurev-genet-110410-132435>.
 44. Tomimatsu N, Mukherjee B, Deland K, Kurimasa A, Bolderson E, Khanna KK, Burma S. 2012. Exo1 plays a major role in DNA end resection in humans and influences double-strand break repair and damage signaling decisions. *DNA Repair (Amst)* 11:441–448. <http://dx.doi.org/10.1016/j.dnarep.2012.01.006>.
 45. Bolderson E, Tomimatsu N, Richard DJ, Boucher D, Kumar R, Pandita TK, Burma S, Khanna KK. 2010. Phosphorylation of Exo1 modulates homologous recombination repair of DNA double-strand breaks. *Nucleic Acids Res* 38:1821–1831. <http://dx.doi.org/10.1093/nar/gkp1164>.
 46. Ismail IH, Gagne JP, Genois MM, Strickfaden H, McDonald D, Xu Z, Poirier GG, Masson JY, Hendzel MJ. 2015. The RNF138 E3 ligase displaces Ku to promote DNA end resection and regulate DNA repair pathway choice. *Nat Cell Biol* 17:1446–1457. <http://dx.doi.org/10.1038/ncb3259>.
 47. Schmidt CK, Galanty Y, Sczaniecka-Clift M, Coates J, Jhujh S, Demir M, Cornwell M, Beli P, Jackson SP. 2015. Systematic E2 screening reveals a UBE2D-RNF138-CtIP axis promoting DNA repair. *Nat Cell Biol* 17:1458–1470. <http://dx.doi.org/10.1038/ncb3260>.
 48. Mischo HE, Hemmerich P, Grosse F, Zhang S. 2005. Actinomycin D induces histone gamma-H2AX foci and complex formation of gamma-H2AX with Ku70 and nuclear DNA helicase II. *J Biol Chem* 280:9586–9594. <http://dx.doi.org/10.1074/jbc.M411444200>.
 49. Craig N. 1973. The effects of inhibitors of RNA and DNA synthesis on protein synthesis and polysome levels in mouse L-cells. *J Cell Physiol* 82:133–150. <http://dx.doi.org/10.1002/jcp.1040820202>.
 50. Francia S, Michelini F, Saxena A, Tang D, de Hoon M, Anelli V, Mione M, Carninci P, d'Adda di Fagnagna F. 2012. Site-specific DICER and DROSHA RNA products control the DNA-damage response. *Nature* 488:231–235. <http://dx.doi.org/10.1038/nature11799>.
 51. Wei W, Ba Z, Gao M, Wu Y, Ma Y, Amiard S, White CI, Rendtlew Danielsen JM, Yang YG, Qi Y. 2012. A role for small RNAs in DNA double-strand break repair. *Cell* 149:101–112. <http://dx.doi.org/10.1016/j.cell.2012.03.002>.
 52. Michalik KM, Bottcher R, Forstmann K. 2012. A small RNA response at

- DNA ends in *Drosophila*. *Nucleic Acids Res* 40:9596–9603. <http://dx.doi.org/10.1093/nar/gks711>.
53. Boguslawski SJ, Smith DE, Michalak MA, Mickelson KE, Yehle CO, Patterson WL, Carrico RJ. 1986. Characterization of monoclonal antibody to DNA:RNA and its application to immunodetection of hybrids. *J Immunol Methods* 89:123–130. [http://dx.doi.org/10.1016/0022-1759\(86\)90040-2](http://dx.doi.org/10.1016/0022-1759(86)90040-2).
 54. Skourti-Stathaki K, Proudfoot NJ, Gromak N. 2011. Human senataxin resolves RNA/DNA hybrids formed at transcriptional pause sites to promote Xrn2-dependent termination. *Mol Cell* 42:794–805. <http://dx.doi.org/10.1016/j.molcel.2011.04.026>.
 55. Suraweera A, Becherel OJ, Chen P, Rundle N, Woods R, Nakamura J, Gatei M, Criscuolo C, Filla A, Chessa L, Fusser M, Epe B, Gueven N, Lavin MF. 2007. Senataxin, defective in ataxia oculomotor apraxia type 2, is involved in the defense against oxidative DNA damage. *J Cell Biol* 177:969–979. <http://dx.doi.org/10.1083/jcb.200701042>.
 56. Phillips DD, Garboczi DN, Singh K, Hu Z, Leppla SH, Leysath CE. 2013. The sub-nanomolar binding of DNA-RNA hybrids by the single-chain Fv fragment of antibody S9.6. *J Mol Recognit* 26:376–381. <http://dx.doi.org/10.1002/jmr.2284>.
 57. Zhang ZZ, Pannunzio NR, Hsieh CL, Yu K, Lieber MR. 2015. Complexities due to single-stranded RNA during antibody detection of genomic RNA:DNA hybrids. *BMC Res Notes* 8:127. <http://dx.doi.org/10.1186/s13104-015-1092-1>.
 58. Shagin DA, Rebrikov DV, Kozhemyako VB, Altshuler IM, Shcheglov AS, Zhulidov PA, Bogdanova EA, Staroverov DB, Rasskazov VA, Lukyanov S. 2002. A novel method for SNP detection using a new duplex-specific nuclease from crab hepatopancreas. *Genome Res* 12:1935–1942. <http://dx.doi.org/10.1101/gr.547002>.
 59. Zhao Y, Hoshiyama H, Shay JW, Wright WE. 2008. Quantitative telomeric overhang determination using a double-strand specific nuclease. *Nucleic Acids Res* 36:e14.
 60. Dutertre M, Lambert S, Carreira A, Amor-Gueret M, Vagner S. 2014. DNA damage: RNA-binding proteins protect from near and far. *Trends Biochem Sci* 39:141–149. <http://dx.doi.org/10.1016/j.tibs.2014.01.003>.
 61. Polo SE, Blackford AN, Chapman JR, Baskcomb L, Gravel S, Rusch A, Thomas A, Blundred R, Smith P, Kzhyshkowska J, Dobner T, Taylor AM, Turnell AS, Stewart GS, Grand RJ, Jackson SP. 2012. Regulation of DNA-end resection by hnRNPU-like proteins promotes DNA double-strand break signaling and repair. *Mol Cell* 45:505–516. <http://dx.doi.org/10.1016/j.molcel.2011.12.035>.
 62. Richard DJ, Bolderson E, Khanna KK. 2009. Multiple human single-stranded DNA binding proteins function in genome maintenance: structural, biochemical and functional analysis. *Crit Rev Biochem Mol Biol* 44:98–116. <http://dx.doi.org/10.1080/10409230902849180>.
 63. Marechal A, Li JM, Ji XY, Wu CS, Yazinski SA, Nguyen HD, Liu S, Jimenez AE, Jin J, Zou L. 2014. PRP19 transforms into a sensor of RPA-ssDNA after DNA damage and drives ATR activation via a ubiquitin-mediated circuitry. *Mol Cell* 53:235–246. <http://dx.doi.org/10.1016/j.molcel.2013.11.002>.
 64. Alzu A, Bermejo R, Begnis M, Lucca C, Piccini D, Carotenuto W, Saponaro M, Brambati A, Cocito A, Fioani M, Liberi G. 2012. Senataxin associates with replication forks to protect fork integrity across RNA-polymerase-II-transcribed genes. *Cell* 151:835–846. <http://dx.doi.org/10.1016/j.cell.2012.09.041>.
 65. Naim V, Wilhelm T, Debatisse M, Rosselli F. 2013. ERCC1 and MUS81-EME1 promote sister chromatid separation by processing late replication intermediates at common fragile sites during mitosis. *Nat Cell Biol* 15:1008–1015. <http://dx.doi.org/10.1038/ncb2793>.
 66. Ohsawa R, Seol JH, Tyler JK. 2013. At the intersection of non-coding transcription, DNA repair, chromatin structure, and cellular senescence. *Front Genet* 4:136. <http://dx.doi.org/10.3389/fgene.2013.00136>.
 67. Chowdhury D, Choi YE, Brault ME. 2013. Charity begins at home: non-coding RNA functions in DNA repair. *Nat Rev Mol Cell Biol* 14:181–189. <http://dx.doi.org/10.1038/nrm3523>.
 68. Wan G, Mathur R, Hu X, Zhang X, Lu X. 2011. miRNA response to DNA damage. *Trends Biochem Sci* 36:478–484. <http://dx.doi.org/10.1016/j.tibs.2011.06.002>.
 69. Gao M, Wei W, Li MM, Wu YS, Ba Z, Jin KX, Liao YQ, Adhikari S, Chong Z, Zhang T, Guo CX, Tang TS, Zhu BT, Xu XZ, Mailand N, Yang YG, Qi Y, Rendtlew Danielsen JM. 2014. Ago2 facilitates Rad51 recruitment and DNA double-strand break repair by homologous recombination. *Cell Res* 24:532–541. <http://dx.doi.org/10.1038/cr.2014.36>.
 70. Aymard F, Bugler B, Schmidt CK, Guillou E, Caron P, Briois S, Iacovoni JS, Daburon V, Miller KM, Jackson SP, Legube G. 2014. Transcriptionally active chromatin recruits homologous recombination at DNA double-strand breaks. *Nat Struct Mol Biol* 21:366–374. <http://dx.doi.org/10.1038/nsmb.2796>.
 71. Gong F, Chiu LY, Cox B, Aymard F, Clouaire T, Leung JW, Cammarata M, Perez M, Agarwal P, Brodbelt JS, Legube G, Miller KM. 2015. Screen identifies bromodomain protein ZMYND8 in chromatin recognition of transcription-associated DNA damage that promotes homologous recombination. *Genes Dev* 29:197–211. <http://dx.doi.org/10.1101/gad.252189.114>.
 72. Wei L, Nakajima S, Bohm S, Bernstein KA, Shen Z, Tsang M, Levine AS, Lan L. 2015. DNA damage during the G0/G1 phase triggers RNA-templated, Cockayne syndrome B-dependent homologous recombination. *Proc Natl Acad Sci U S A* 112:E3495–E3504. <http://dx.doi.org/10.1073/pnas.1507105112>.
 73. Keskin H, Shen Y, Huang F, Patel M, Yang T, Ashley K, Mazin AV, Storici F. 2014. Transcript-RNA-templated DNA recombination and repair. *Nature* 515:436–439. <http://dx.doi.org/10.1038/nature13682>.
 74. Shen Y, Nandi P, Taylor MB, Stuckey S, Bhadsavle HP, Weiss B, Storici F. 2011. RNA-driven genetic changes in bacteria and in human cells. *Mutat Res* 717:91–98. <http://dx.doi.org/10.1016/j.mrfmmm.2011.03.016>.
 75. Yang YG, Qi Y. 2015. RNA-directed repair of DNA double-strand breaks. *DNA Repair (Amst)* 32:82–85. <http://dx.doi.org/10.1016/j.dnarep.2015.04.017>.
 76. Meers C, Keskin H, Storici F. 2016. DNA repair by RNA: templated, or not templated, that is the question. *DNA Repair (Amst)* 44:17–21. <http://dx.doi.org/10.1016/j.dnarep.2016.05.002>.
 77. Yang Q, Jankowsky E. 2005. ATP- and ADP-dependent modulation of RNA unwinding and strand annealing activities by the DEAD-box protein DED1. *Biochemistry* 44:13591–13601. <http://dx.doi.org/10.1021/bi0508946>.
 78. Rossler OG, Straka A, Stahl H. 2001. Rearrangement of structured RNA via branch migration structures catalysed by the highly related DEAD-box proteins p68 and p72. *Nucleic Acids Res* 29:2088–2096. <http://dx.doi.org/10.1093/nar/29.10.2088>.